Yin et al. *NPG Asia Materials* (2024)16:8
https://doi.org/10.1038/s41427-023-00513-9

NPG Asia Materials

REVIEW ARTICLE Open Access

Wearable respiratory sensors for health monitoring

Zhifu Yin[1,2,3], Yang Yang[1], Cong Hu[3], Jinzhe Li[1,4], Boyu Qin[2] and Xue Yang[1,5]

Abstract

Real-time monitoring and early warning of human health conditions is an important function of wearable devices. Along with the development of the Internet of Things and the medical drive for early detection and treatment, wearable devices will become increasingly important in the future. Compared with traditional sensors, wearable sensors with mechanical softness and deformability are able to adapt to geometric nonlinearities and deformations caused by motion that occurs in application scenarios, thus ensuring stable and effective signal output under various complex working conditions. Various novel sensing materials have been developed for the detection of various biomarkers of respiration over the past few years. Here, we summarize the latest innovations in wearable respiratory sensors, highlighting the dominant sensing materials, designs, sensing mechanisms, and clinical implications. Finally, the future challenges and directions of wearable respiratory sensors are outlined toward promoting advancement in the field of wearable respiratory monitoring.

Introduction

With a growing population, increasing aging and frequent threats to global safety, public healthcare systems are under increasing pressure and are experiencing a significant shift from traditional hospital-centric systems to individual-centric systems. Wearable devices, as a new tool in human-computer interaction, can provide the human body with physical signals such as respiratory rate, pulse, and exercise status, as well as chemical signals such as blood glucose and volatile organic compounds (VOCs). These signals can be conveniently and simply transmitted to a host computer via radio frequency identification (RFID) tags, Bluetooth, or simple data lines and can be used as a basis for evaluation and diagnosis.

The use of exhaled gases for disease diagnosis is an ancient practice. In the late 1780s, Lavoisier took the first initiative to determine the chemical components of human breath, and in 1971, Linus Pauling demonstrated that breath is a complex gas containing no less than 200 VOCs. More recently, respiratory analysis has shown noninvasive and extraordinary promise as a modality for clinical diagnosis, disease state monitoring, and environmental exposure assessment[1,2]. Human exhaled breath mostly contains nitrogen [78.04%], oxygen [16%], carbon dioxide [4–5%], hydrogen [5%], inert gases [0.9%] and water vapor. In addition, exhaled gas contains a variety of inorganic compounds in parts-per-billion (ppb) or parts-per-million (ppm) concentrations, including nitric oxide [10–50 ppb], nitrous oxide [1–20 ppb], ammonia [0.5–2 ppm], carbon monoxide [0–6 ppm], and hydrogen sulfide [0–1.3 ppm]. VOCs such as acetone [0.3–1 ppm], ethanol, isoprene [~105 ppb], ethane [0–10 ppb], methane [2–10 ppm], and pentane [0–10 ppb][3,4]. can also be found in exhaled gases.

As a noninvasive test, breath testing offers exciting advantages: the breath test is completely noninvasive and even nonsensitive, greatly reducing the pain and inconvenience of testing compared to traditional testing methods (blood tests, urine tests). Compared to other noninvasive testing (sweat, tears, interstitial fluid, etc.) methods, exhaled gas is not only easy and quick to obtain but also available in sufficient quantity, especially for respiratory-related diseases, where breath testing can provide direct information that all other tests do not. By measuring the concentration of specific biomarkers in exhaled breath, it is possible to determine the health status and degree of disease of an individual and provide guidance for treatment.

Correspondence: Xue Yang (yangxJLU@aliyun.com)
[1]School of Mechanical and Aerospace Engineering, Jilin University, Changchun 130025, China
[2]State Key Laboratory of Electrical Insulation and Power Equipment, Xi'an Jiaotong University, Xi'an 710049, China
Full list of author information is available at the end of the article

Combining respiratory sensors with flexible wearable device manufacturing technology to develop wearable respiratory devices can achieve continuous noninvasive monitoring of human health[5]. In addition, the detection of respiratory rate or exhaled breath condensate (EBC) is also an important direction. Continuous measurement of respiratory rate provides convenient insight into the subject's breathing status over a period of time, which can guide the extent of disease progression, such as for sleep apnea, asthma and chronic obstructive pulmonary disease. Airway lining fluids contain antioxidants, soluble markers and other biochemical molecules that can be exhaled with gas during calm breathing. These substances condense with water vapor under cold conditions to form EBC, which can also be used for routine health monitoring by measuring the concentration of biomarkers in EBC.

Sensors determine the performance of wearable devices and are the most important component of wearable devices. This review discusses the achievements of wearable gas sensors in recent years, as well as physiological/pathological parameters related to exhaled gases. The first chapter describes the main sensing materials applied to gas sensors, as well as the characteristics and preparation of these materials. Chapter 2 summarizes the sources of biomarkers in exhaled gas and the correspondence between biomarkers and diseases as well as wearable devices used for biomarker detection in recent years. Chapter 3 provides an overview of the opportunities and challenges of wearable respiratory sensors for health care applications (Fig. 1).

Introduction to wearable devices

Sensing materials

Respiratory sensors are the "brains" of respiratory wearable devices and play a vital role in respiratory monitoring. To achieve the desired goal, wearable respiratory sensors need to meet the following conditions: capable of responding quickly and accurately to target biomarkers in exhaled gas at room temperature; the sensing material is nontoxic, can be easily manufactured, is robust to large mechanical deformations, and is insensitive to small deformations. Traditional gas sensing materials are rigid semiconductors and conductors. However, higher sensing temperatures, as well as the inherent brittleness and stiffness of the materials, limit their use in wearable respiratory sensors. With the development of materials science, various nanomaterials have been discovered, fabricated, and applied in different scenarios. In this section, we discuss five categories of sensing materials, i.e., semiconducting metal oxides, C-based materials, hybrid nanomaterials, conductive polymers, and other materials. Figure 2 shows some of the achievements in the development of wearable gas sensing materials.

Semiconductor metal oxide (SMO)

In recent decades, SMO-based chemiresistive sensors have shown great potential for disease detection and health monitoring based on volatile human exhalation[6,7]. The reversible interaction of gases with material surfaces is the basis for the application of SMO-based gas sensors[1,8]. Based on the relationship between the valence band, forbidden band, and conduction band, SMO can be classified into two major categories: n-type SMO and p-type SMO.

N-type SMO is also known as electronic-type SMO (e.g., SnO_2, ZnO, In_2O_3, WO_3 and Fe_2O_3), jumping of electrons from the donor band to the conduction band at high temperature, and the carriers are free electrons. P-type SMO is also known as hole-type SMO (e.g., NiO, CuO, Cr_2O_3, Co_3O_4, and $Mn_3O_{4)}$, and the electrons of p-type semiconductors jump from the valence band to the host band at high temperatures and leave the holes as carriers. The addition of electrons in the conduction band and the leaving holes in the valence band both increase the number of carriers in the material, which manifests as an increase in the conductivity of the semiconductor. Thus, at room temperature, SMO behaves as an insulator, while in high-temperature environments, it behaves as a conductor.

There is a large amount of oxygen in the air (approximately 21% of the air). Oxygen has a high electronegativity and can easily react with semiconductor materials to form oxygen ions wrapped around the surface of the material, exhibiting the generation of an electron depletion layer (EDL) and hole accumulation layer (HAL) in n-type and p-type semiconductors, respectively. When the sensor contacts oxidizing gases (e.g., Cl_2, NO_x, SO_2, etc.), the oxygen ions on the sensor surface oxidize them and absorb electrons from the EDL or HAL, causing an increase in the EDL and HAL, which appears as a decrease in the conductivity of an p-type semiconductor and an increase in the conductivity of an n-type semiconductor. The higher the concentration of the reactive gas is, the greater the change in the resistance of the sensing material. When the reducing gas is removed, the material returns to its original properties. When SMO is exposed to reducing gases (e.g., CO, H_2, CH_3, ethanol, acetone, etc.), the exact opposite of the above reaction occurs, i.e., the EDL and HAL decrease, which appears as an increase in the electrical conductivity of a p-type semiconductor and a decrease in the electrical conductivity of an n-type semiconductor[9]. A graphical representation of the change in electrical conductivity of an SMO material is shown in Fig. 3.

Many efforts have worked on improving the sensing performance of SMO sensors. Since the SMO gas sensing mechanism is mainly due to the oxidation/reduction reactions occurring between the gas and the surface of the

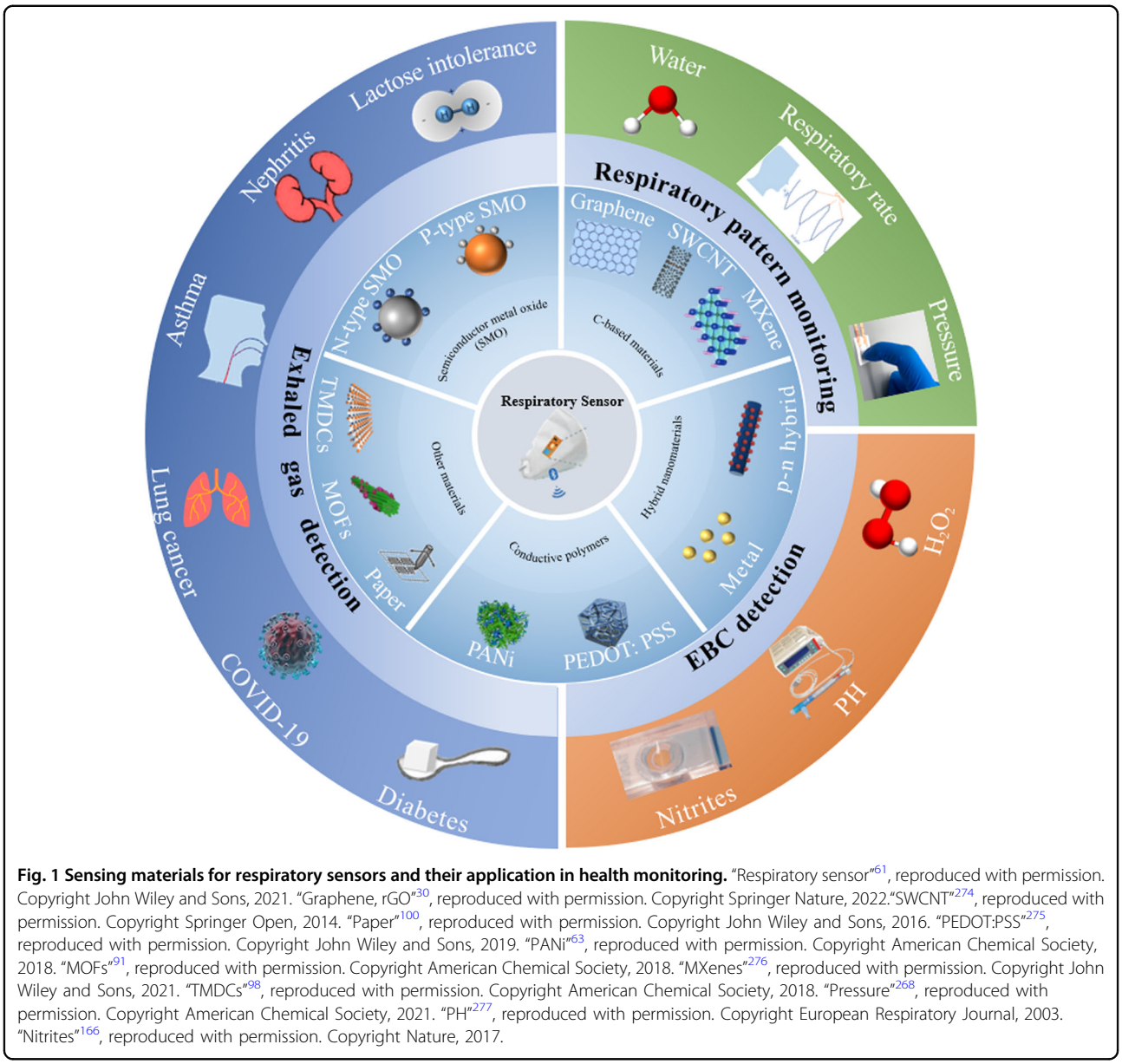

Fig. 1 Sensing materials for respiratory sensors and their application in health monitoring. "Respiratory sensor"[61], reproduced with permission. Copyright John Wiley and Sons, 2021. "Graphene, rGO"[30], reproduced with permission. Copyright Springer Nature, 2022."SWCNT"[274], reproduced with permission. Copyright Springer Open, 2014. "Paper"[100], reproduced with permission. Copyright John Wiley and Sons, 2016. "PEDOT:PSS"[275], reproduced with permission. Copyright John Wiley and Sons, 2019. "PANi"[63], reproduced with permission. Copyright American Chemical Society, 2018. "MOFs"[91], reproduced with permission. Copyright American Chemical Society, 2018. "MXenes"[276], reproduced with permission. Copyright John Wiley and Sons, 2021. "TMDCs"[98], reproduced with permission. Copyright American Chemical Society, 2018. "Pressure"[268], reproduced with permission. Copyright American Chemical Society, 2021. "PH"[277], reproduced with permission. Copyright European Respiratory Journal, 2003. "Nitrites"[166], reproduced with permission. Copyright Nature, 2017.

sensing material[10], better sensing performance can be achieved in several ways:

i. Adjusting the size of the material. Jin et al.[11] controlled the concentration of the precursor solution to fabricate α-Fe_2O_3 nanoparticles with different grain sizes and then compared their sensor responses to ethanol gas. Finally, they found that the sensor response increases up to a grain size of 15.9 ± 1.4 nm and then decreases with a further increase in grain size.
ii. Tuning the nanostructure of materials. The lower the dimensionality of the material is, the larger the specific surface area and therefore the more binding sites will be available. The 0-dimensional form has been introduced in the discussion of sensing principles. A 1-dimensional morphology means that two of the three dimensions of the material (x, y, z) are in the range of 0.1–100 nm. In recent years, through technologies such as electrostatic spinning, stencil printing and vapor-liquid–solid growth, researchers have fabricated various wire-like materials (nanowires, nanorods, nanotubes, etc.) with controlled morphology and composition for the detection of specific gases at room temperature. A 2-dimensional morphology indicates that one of the three dimensions of the material (x, y, z) is in the range of 0.1–100 nm and mainly refers to various sheet-like structures.

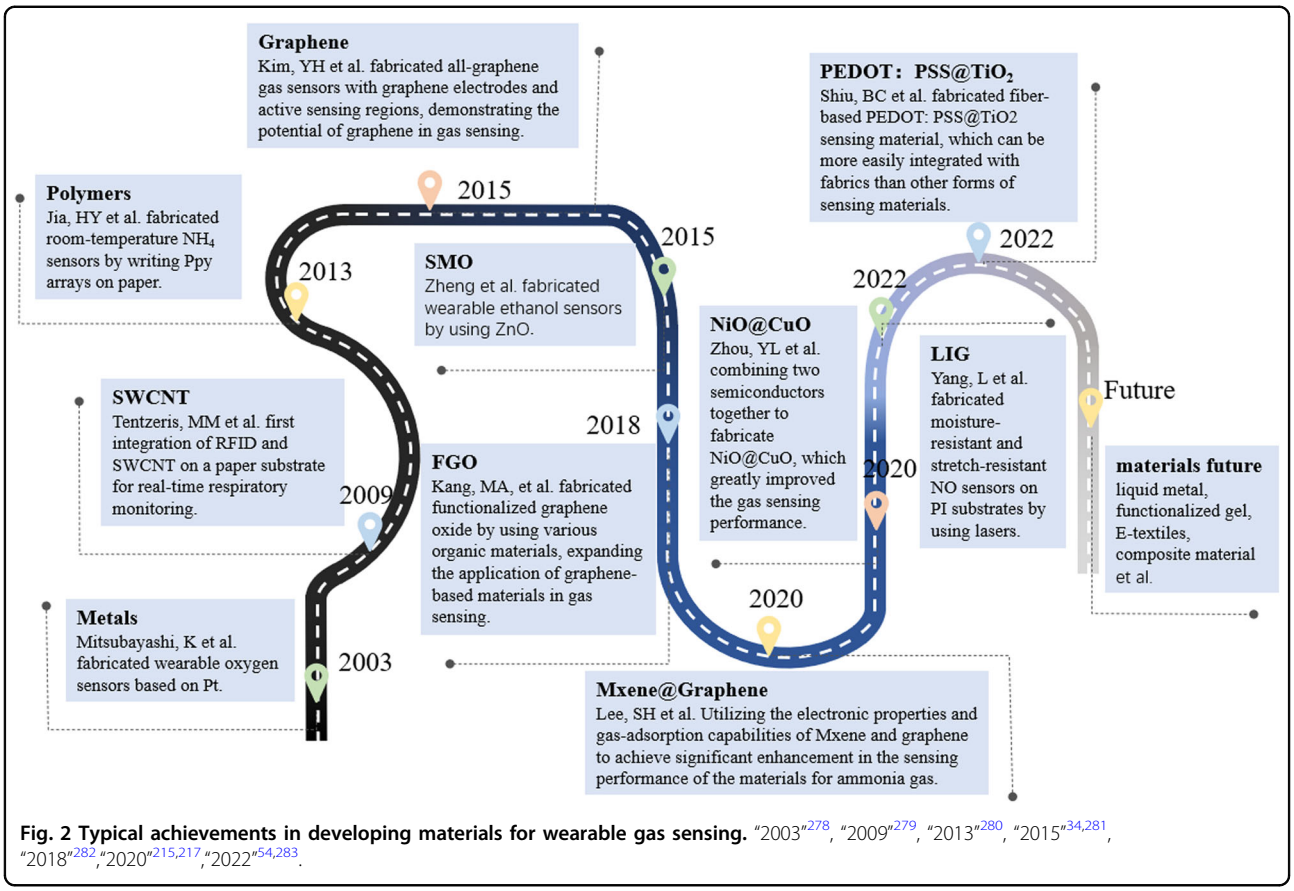

Fig. 2 Typical achievements in developing materials for wearable gas sensing. "2003"[278], "2009"[279], "2013"[280], "2015"[34,281], "2018"[282], "2020"[215,217], "2022"[54,283].

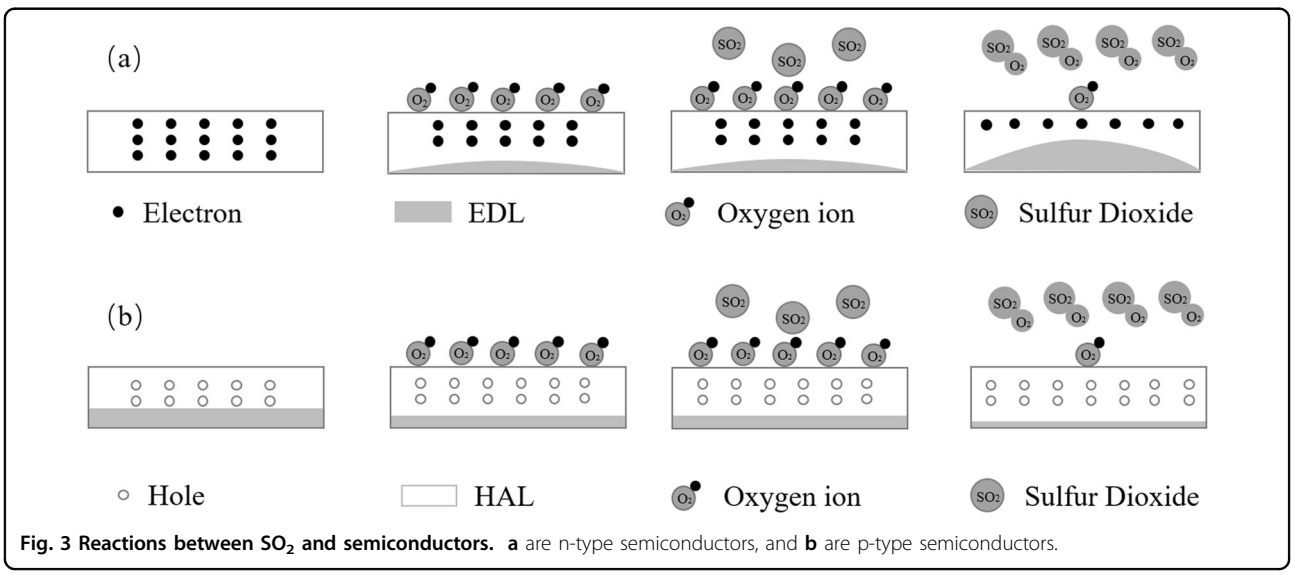

Fig. 3 Reactions between SO_2 and semiconductors. **a** are n-type semiconductors, and **b** are p-type semiconductors.

Notably, nanotubes are also considered to be nanosheets in a rolled up state and are thus considered to be 2D materials in some studies. Typical 2D materials include graphene, black phosphorus (BP), 2D transition metal dichalcogenides (TMDCs), 2D transition metal carbides, carbonitrides, and nitrides. Due to their chemical, physical and thermal stability and planar crystal structure characteristics, these two-dimensional (2D) materials have proven

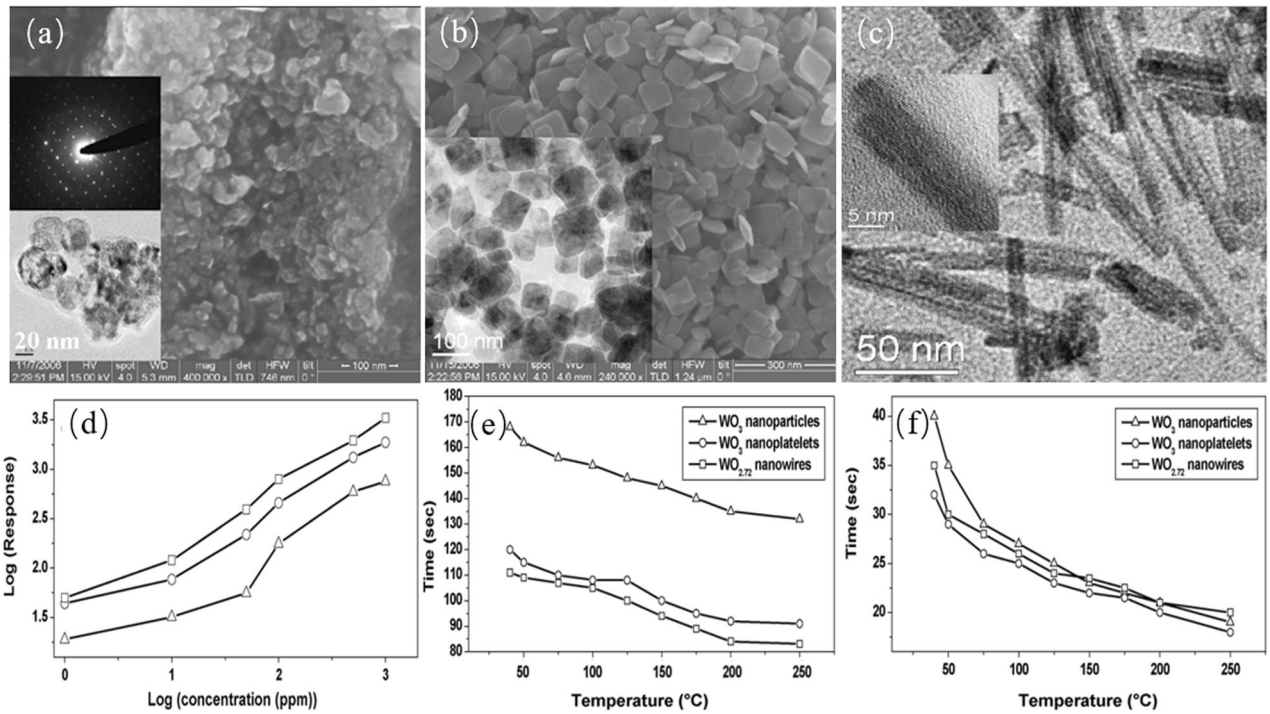

Fig. 4 Differences in the H_2S response of WO_3 with different nanostructures. FESEM images of **a** tungsten oxide nanoparticles with the inset showing a TEM image and electron diffraction and **b** tungsten oxide nanoplatelets with the inset showing a TEM image, **c** A TEM image of $WO_{2.72}$ nanowires with the inset showing an HREM image. **d** A comparison of the response values of tungsten oxide nanostructures with H_2S concentration (at 250 °C), temperature variation of **e** response and **f** recovery times (to 1000 ppm H_2S) of tungsten oxide nanoparticles, nanoplatelets and nanowires. Reproduced with permission from ref. [12]. Copyright Elsevier, 2008.

advantageous in sensing applications. Rout et al.[12], by studying the response of different nanostructures of WO_3 to H_2S, it is clearly shown that the sensitivity of WO_3 nanowires (3313) is much higher than that of WO_3 nanosheets (1852), and the nanosheet structure is in turn more sensitive than that of spherical WO_3 nanoparticles (757) (Fig. 4).

iii. Increasing the porosity of the material. For example, materials are fabricated into structures such as core-shells and hollow porous structures, which allow gases to easily enter and exit the interior of the structure and interact with each other, increasing the material S/V and improving the surface active site, resulting in a large improvement in material sensing performance[13,14]. Xu et al.[15] used SiO_2 nanoparticles and polyvinylpyrrolidone (PVP) as sacrificial templates and synthesized mesoporous WO_3 fibers by electrostatic spinning in the aqueous phase. The room-temperature gas sensor fabricated from this material can detect acetone vapor at <1 ppm with good linearity and selectivity. The traditional spherical structure is considered an unfavorable morphology in sensing, but by changing the morphology of the hollow porosity, the sensor performance can be substantially improved. Jang et al.[14] used materials such as apoferritin, polystyrene (PS), Pt^{4+} ions, and SnO_2 and prepared nanoporous Pt-PS_SnO_2 NTs by electrostatic spinning and high-temperature thermal decomposition, which showed an extremely high response to acetone gas as well as excellent selectivity and were able to achieve acetone detection at a minimum of 10 ppb. Yoon et al.[16] synthesized 3 M-SnO_2 materials with macro, meso-, and micropores, allowing gases to flow in macro, meso-, and micropores with different diffusion mechanisms, such as normal diffusion, Knudsen diffusion, and surface diffusion, respectively. These materials can respond to ethanol at the ppb level. Figure 5 shows some typical work to increase the porosity of materials.

C-based materials

Carbon-based nanomaterials such as carbon nanofibers, carbon nanotubes, graphene oxide (GO), and graphene have excellent physical and chemical properties (e.g., high carrier mobility, mechanical robustness, and large surface area). Compared with conventional conductive materials

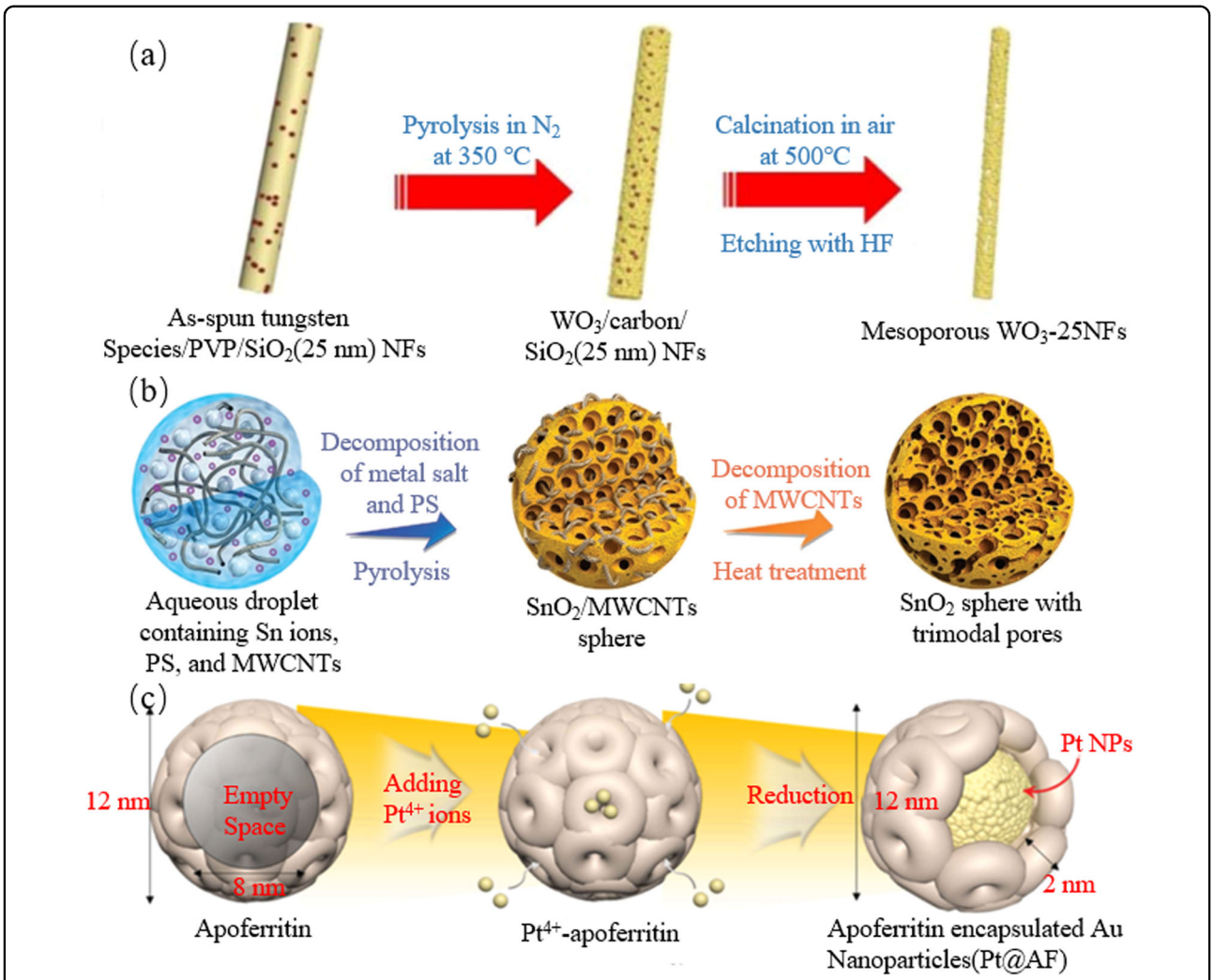

Fig. 5 Typical work to increase the porosity of materials. a The fabrication process of the mesoporous WO_3 NFs. Reproduced with permission from ref. [15]. copyright frontiers, 2019. **b** The formation of SnO_2 nanospheres with trimodal porosity. Reproduced with permission from ref. [16]. Copyright Nature, 2016. **c** Synthetic process for apoferritin-encapsulated catalytic NPs. Reproduced with permission from ref. [14]. Copyright John Wiley and Sons, 2019.

(e.g., ITO, Si, Ge, GaAs, etc.), C-based materials exhibit better flexibility and gas sensing performance at room temperature. Unlike the sensing mechanism of SMO, the adsorption of target gas molecules with C-based materials such as graphene, CNTs, and MXenes does not require the action of oxygen ions in air. Compared with traditional conductive materials (such as ITO, Si, Ge, and GaAs), C-based materials show better flexibility and good sensing ability at room temperature. The target gas molecules are physically adsorbed on the surface of the sensing material through the van der Waals effect or the donor-recipient interaction and undergo charge transfer at the interface of the two materials, which alters the carrier concentration of the sensing material and leads to a change in the electrical resistance of the sensing material. With in-depth research on C-based materials, the application of these materials in flexible wearable sensors is becoming increasingly widespread. Here, we discuss the characteristics of various C-based materials.

Carbon nanotubes are a unique quasione-dimensional structure, and their molecular structure can be considered as graphene sheets rolled up in a specific direction and specified by a pair of integers (n, m). Carbon nanotubes can be classified into single-walled carbon nanotubes (SWCNTs) and multiwalled carbon nanotubes (MWCNTs) according to their composition. SWCNTs are seamless cylindrical tubes with a diameter of a few nanometers and a length of 0–100 μm, obtained by convolving graphene along a selected axis. The chiral vector of SWNTs is characterized by a pair of indices (n, m) and determines their conductivity. As a common opinion, when $m = 0$, the nanotubes are named zigzag nanotubes,

and their conductivity behaves as a semiconductor. When n = m, the nanotubes are named armchair nanotubes, their conductivity behaves as a conductor, and other states are denoted chiral nanotubes, and they have semiconducting properties[9,17,18]. SWCNTs are often used as a sensing material for NO_2 and NH_3 gas sensors due to their low resistivity, high carrier mobility, high mechanical strength and specific response to specific substances. Agarwal et al.[19] prepared a chemiresistive flexible NO_2 gas sensor by spray coating dispersion-treated SWCNTs on a polytetrafluoroethylene (PTFE) membrane, which has high sensitivity to dry NO_2 gas at room temperature in the concentration range of 0.75 ppm ~ 5 ppm for a response of 21.58% ~ 167.7%. CNTs interact with target gases either by van der Waals or donor–acceptor interactions[20]. Experiments and studies have shown the adsorption of gas molecules on the surface of SWCNTs, especially at defective spots[21,22]. Therefore, the controlled introduction of defects can increase the chemical selectivity and sensitivity of SWCNTs[23]. Of course, the introduction of defects reduces the electron transport capacity of SWCNTs, so a balance must be struck between the defect concentration and the electronic properties of SWCNTs to obtain the best performance.

Graphene is a thin sheet-like two-dimensional nanomaterial with a honeycomb structure of sp^2-hybridized carbon atoms, often characterized as a p-type semiconductor, and has received widespread worldwide attention for its excellent properties. Graphene nanosheets were first separated by mechanical exfoliation using simple adhesive tape[24]. Since then, several synthetic routes have been used to prepare graphene layers and thin films, including chemical vapor deposition (CVD)[25], liquid-phase mechanical exfoliation of graphite[26], graphite intercalation compounds[27], epitaxial growth[28], and atomic layer etching (ALE)[29]. Graphene consists of a single layer of carbon atoms, allowing all carbon atoms to interact directly with the analyte[30], and has a very high carrier mobility; namely, the conducting electrons in graphene can transport rapidly through the lattice (up to 350,000 $cm^2/(V\ s)$), at a much faster rate than metal conductors[31]. Graphene has a high optical transparency, with a single layer capable of reaching over 97.7% transmittance[32]. Graphene also has high thermal conductivity, with the thermal conductivity of monolayer graphene ranging from 4.84 to 5.30 KW/m K at room temperature[30]. However, pristine graphene has almost no dangling bonds on its surface, which results in poor graphene sensing performance in terms of both speed and selectivity for the target gas at room temperature. To improve the sensing properties of pristine graphene, many studies have proposed different approaches. Ma et al.[33] introduced defective graphene into pristine graphene to increase the binding sites of the material to the target gas, resulting in a 13-fold higher response to NO_2 than pristine graphene. Kim et al.[34] proposed an all-graphene-based NO_2 sensor, in which the response and recovery times were drastically reduced by increasing the bias voltage and the operating temperature of the all-graphene sensor.

Graphene can be oxidized to GO sheets containing oxygen-containing functional groups (OCFGs), such as carboxyl (−COOH), hydroxyl (−OH), epoxy (C−O−C), carbonyl (−C−OH), ketone (−C=O), and 5- and 6-membered ring lactols (O–C−O), by the action of some acids[32,35,36]. Due to the incorporation of OCFGs, GO exhibits a number of physical and chemical properties that are quite different from those of graphene: GO exhibits hydrophilicity and can be used to make humidity sensors[37]. The OCFGs of GO also provide the basis for surface functionalization, and surface-functionalized GO exhibits enhanced sensitivity and selectivity for some specific substances and has been used to fabricate various sensors for some specific substances[38,39]. However, the low thermal and electrical conductivity of GO hinders its wide application in electronic devices.

The OCFGs of GO can be removed by chemical reduction using reducing agents such as hydrazine, sodium borohydride, glucose, and hydroquinone in the solution state or by thermal reduction in the solid-state through annealing, using electrochemical methods, or laser irradiation, which can convert GO into reduced graphene oxide (rGO) and significantly improve its properties, such as thermal conductivity, mechanical strength, and electron mobility[40–42]. rGO can be easily fabricated by the process of oxidizing and then reducing graphite, which solves the problems of difficult graphene fabrication and poor selectivity to specific substances and significantly improves the electrical conductivity compared to GO, so rGO is more widely used as a sensitive material for wearable flexible sensors at room temperature[43–45]. Figure 6 shows the classical structures of graphene and CNTs.

Laser-induced graphene (LIG) is a new graphene fabrication technique that utilizes a laser beam to induce a photothermal reaction in a tiny area. These carbon precursor materials absorb the energy of the incoming photons, and the rapid energy deposition generates high temperatures locally sufficient to break the chemical bonds, after which the carbon atoms rearrange themselves into graphene. Patterned graphene can thus be fabricated in a single step by laser scribing on the surface of some commercially available polymer films (e.g., polyimide (PI) polyetherimide (PEI)) under natural environmental conditions[46–48]. By adjusting the laser output parameters, irradiation environment and other conditions, LIGs with different physical morphologies and electrical and chemical properties can be fabricated (Fig. 7d), and there are

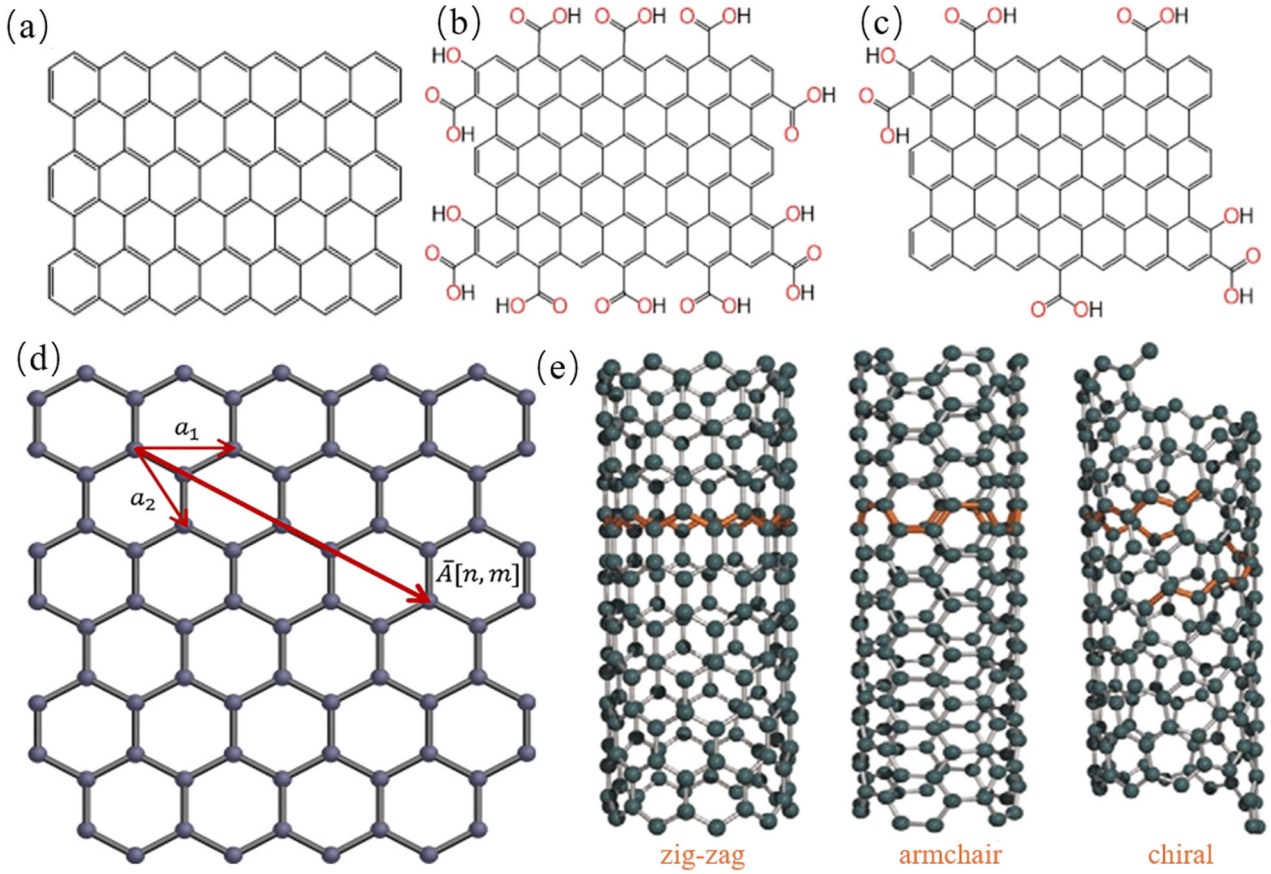

Fig. 6 The classical structures of graphene and CNTs. Molecular structure of **a** graphene, **b** graphene oxide, and **c** reduced graphene oxide. Reproduced with permission from ref. [30]. **d** Carbon nanotube chiral vector, reproduced with permission from ref. [9]. Copyright Elsevier, 2018. **e** Models of three atomically perfect SWNT structures. Reproduced with permission from ref. [274].

significant differences in properties across the LIGs generated under different conditions[49–53]. Yang et al.[54] prepared moisture-resistant and stretchable NO_x gas sensors by adjusting the conditions of power, image density and defocus distance of the laser. The gas sensor enabled monitoring an individual's local environment at different times of the day and analyzing human breath samples to classify patients with respiratory diseases from healthy volunteers. In addition, LIG can even be generated on natural substrates (potato skins, coconut shells, cork, etc.) by means of scattered focus and multiple laser irradiation[55]. Compared with other manufacturing methods of graphene, using laser engraving to generate graphene in a single step saves high-temperature processing or multiple chemical synthesis steps, and the properties of the fabricated LIG are highly tunable, providing a new solution for the manufacture and application of graphene.

2D transition metal carbides, carbonitrides, and nitrides, namely, MXenes, have emerged as a promising family of 2D nanomaterials since their first report in 2011[56]. MXenes are typically synthesized by a top-down selective etching procedure of the ternary precursor MAX, where M represents a transition metal (Sc, Ti, Zr, Hf, etc.), A usually belongs to the IIIA or IVA groups, and X is carbon and/or nitrogen that is connected with layers of A atoms[57]. MXenes share a general structure similar to $M_{n+1}X_nT_x$, in which M denotes the early transition metal (e.g., M refers to Sc, Ti, V, Cr, Y, Zr, Nb, Mo, Hf, Ta, W, etc.), X refers to C/N/CN, n can be 1, 2, 3, or 4, and T_x signifies the surface terminations (e.g., T refers to O, OH, F, Cl, I, Br, S, Se, or Te, etc.) on the outer surface of the chemically active transition metal layers (the subscript x in T_x is a variable denoting the number of surface functionalities)[58–60]. Due to their tunable interlayer spacing, intriguing surface chemistry, and other physicochemical properties. MXenes have received significant attention recently. Li et al.[61] reduced the hydrophilicity of $Ti_3C_2T_x$ MXenes by introducing hydrocarbon terminations while improving their sensitivity to VOCs and subsequently prepared $Ti_3C_2T_x$-M_2 by alkali pretreatment, from which a wearable wireless ethanol vapor detection tag was prepared that can dynamically track ethanol exhaled after

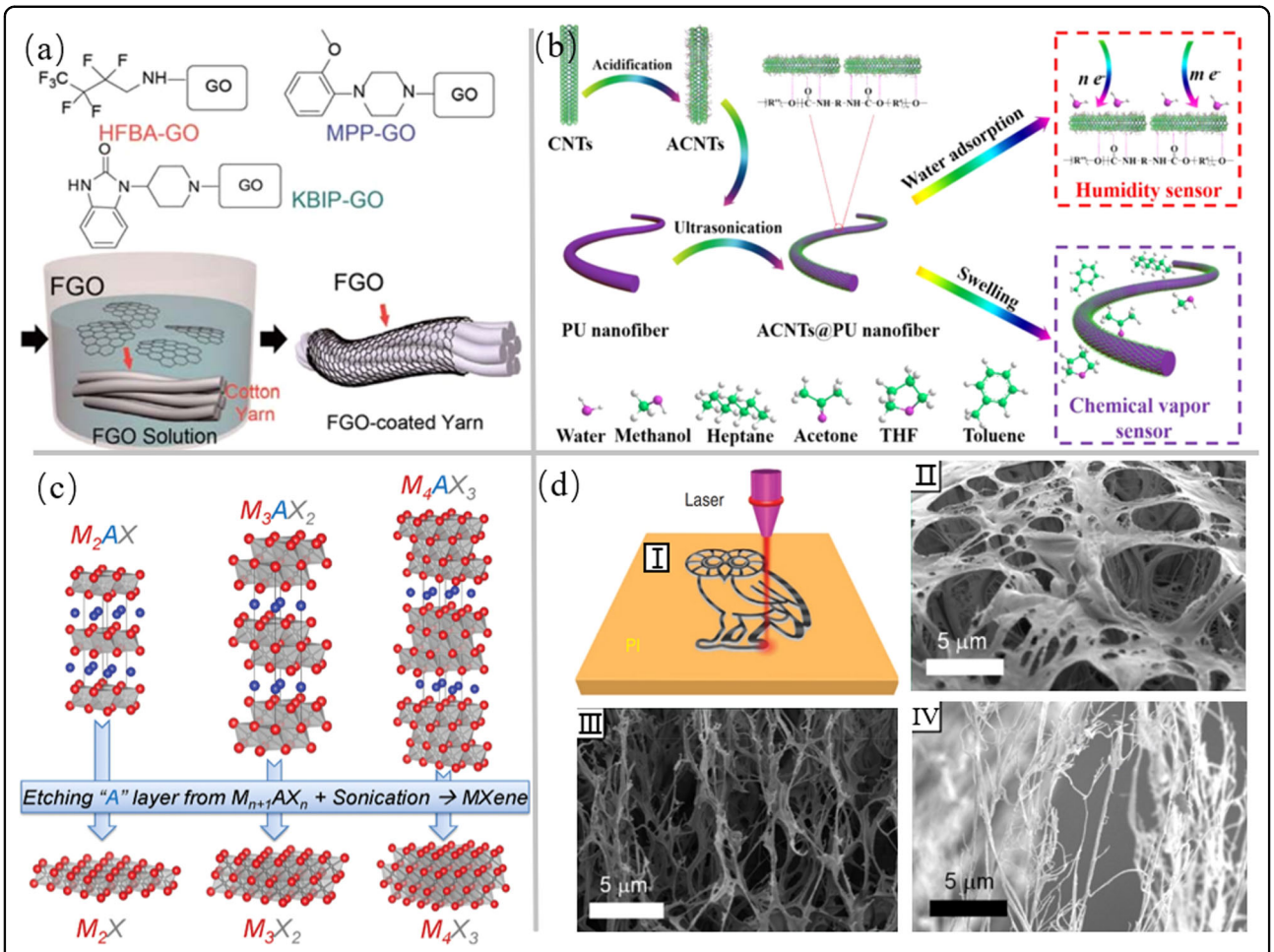

Fig. 7 Novel carbon-based materials. a Schematic diagram of functionalized graphene oxide (FGO) coated on a single yarn for gas detection[282]. Reproduced with permission from ref. [282]. Copyright Royal Society of Chemistry, 2018. **b** Schematic demonstration of the preparation of CNCs and the sensing mechanisms for humidity and chemical vapor sensors. Reproduced with permission from ref. [250]. Copyright American Chemical Society, 2019. **c** Structure of MAX phases and the corresponding MXenes. Reproduced with permission from ref. [58]. Copyright Wiley-VCH, 2014. **d** (I) Schematic of the synthesis process of LIG from PI. Reproduced with permission from ref. [46]. Copyright Nature Publishing Group, 2014. SEM showing the swelling of polyimide at different distances, (II) z = 3 mm, (III) z = 1.8 mm, (IV) z = 0 mm. Reproduced with permission from ref. [52]. Copyright American Chemical Society, 2021.

alcohol intake as well as distinguish alcohol breath from normal breath. Xing et al.[62] converted pristine fabric into an MXene/MWCNT fabric by using a simple alternating drop coating and integrated MXene/MWCNT fabric sensors into a wireless flexible detection tag and inserted it into a mask for exhaled gas humidity detection. The wearable MXene/MWCNT fabric humidity sensor can accurately detect each tidal breath and determine the breathing status (normal breath, fast breath, slow deep breath and apnea), which provides a feasible method for real-time breath analysis. Figure 7 presents novel materials in carbon-based materials.

Conductive polymers

Conductive polymers, such as polyaniline (PANi), poly(3,4-ethylenedioxythiophene):poly(styrenesulfonate) (PEDOT:PSS), polypyrrole (PPy), poly(4-vinylpyridine) (P4VP) and its derivative polystyrene (PS), have promising applications as flexible wearable sensors in the sensing field due to their mechanical robustness, convenient doping with various sensing materials, easy adjustment to different nanostructures, and favorable sensing capability at room temperature.

Among conductive polymers, PANi is an excellent sensing material due to its easy synthesis, high sensitivity, high electrical stability, unique doping properties, high electrical conductivity and reversible redox reaction. The most common oxidation states of polyaniline are light emeraldine, near-nitroaniline and emeraldine. In addition, emeraldine can be synthesized into two forms: emeraldine salt (ES) and emeraldine base (EB), of which only ES has a semiconductor-scale electrical conductivity at room

temperature; the others are insulators, and using this property, polyaniline can be used as a means of detection for some gases. Kang et al.[63]. doped p-toluene sulfonate hexahydrate (PTS) with PANi as a sensing material and fabricated a near-field communication (NFC) tag for ammonia gas by inkjet printing. The principle that PTS −PANi is dedoped into its EB form from its ES form by interaction with alkali gas, thus causing an increase in resistance, is used to achieve highly sensitive detection of ammonia. However, the poor chemical stability and mechanical strength of PANi at higher temperatures remain a challenge for its practical application as a favorable sensing material. Many methods have been implemented to solve these problems, such as the introduction of inorganic metal oxides into PANi during the synthesis process. To date, several metal oxide (such as ZnO, CeO_2, TiO_2, SnO_2 and WO_3) nanostructures have been synthesized into PANi by aniline chemical oxidation polymerization, inverse micellar polymerization, hydrothermal methods, layer-by-layer (LbL) self-assembly methods, sol-gel techniques, etc. Liu et al.[64] investigated the effect of nano-CeO_2 on aniline polymerization by comparing the morphological, structural and chemical characteristics of pure PANi and PANi-CeO_2 nanocomposites and found that PANi is significantly more protonated and oxidized in PANi-CeO_2 nanocomposites. Meanwhile, the NH_3 sensing performance of the PANi-CeO_2 thin film sensor was significantly enhanced at room temperature (~25 °C), and the results showed that the PANi-CeO_2 thin film sensor has a higher response, shorter recovery time, and ultralow detection concentration (16 ppb). Figure 8 presents the application of PANi in gas sensing.

PEDOT:PSS is a well-known conductive polymer that is water dispersible and commercially available. Its chemical stability and highly adjustable conductivity have also been studied for the accurate detection of various gases at room temperature. Li et al.[65] used PEDOT:PSS as the active layer and added optimized concentrations of silver nanowires to PEDOT:PSS films to obtain the sensitive material PEDOT:PSS/AgNW, which was used to prepare a flexible NH_3 sensor on a PET substrate. The resulting sensor had excellent ammonia sensing performance at room temperature and was capable of detecting NH_3 at concentrations below 500 ppb.

Hybrid nanomaterials

This section describes materials that are often mixed together, such as metal and C-based materials, different types of SMO, metal oxides and conductive polymers. In the study of gas sensing materials, metal nanoparticles are often doped onto sensing materials to enable various functionalization[66–69]. Metal molecules have a crystalline structure (face-centered cubic (FCC), body-centered cubic (BCC) and hexagonal close packed HCP), and precious metals such as gold, platinum, palladium and silver are FCC crystal structures. Precious metals offer the advantages of high electrical conductivity, high melting point, and high oxidation resistance, especially their efficient oxygen decatalysis capability[1,70,71], which makes them widely used in gas sensing. However, none of the metals except palladium have specific selectivity for gases, so none of these metals can be used directly as sensitive materials for gas sensing.

Palladium can absorb 900 times its volume of hydrogen at room temperature, so palladium can be used alone as a sensing material for hydrogen[72]. Theoretical studies explain the reaction mechanism of the specific binding of palladium to hydrogen: palladium can decompose the hydrogen molecules adsorbed on its surface into two hydrogen atoms, which, by diffusion, occupy the void positions of the palladium lattice, causing the expansion of the palladium lattice, generating PdHx hybridization and causing changes in the physical properties of palladium, including mass, electrical conductivity, and volume. Thus, the hydrogen concentration can be evaluated both by the increase in resistance of the palladium film exposed to hydrogen and by the increase in conductivity of the discontinuous palladium layer due to expansion[9,73]. Although several studies have reported on H_2 sensors made of pure palladium, these sensors still have non-negligible defects that affect their use in gas sensing: under low H_2 concentrations down to 7 Torr at 300 K, the α-hybrid generated by Pb at low hydrogen concentrations (<200 ppm) is converted to the β-hybrid generated at high hydrogen concentrations (>5000 ppm), and the process is irreversible. In addition, the response time of these sensors is typically at least a few minutes and does not meet the need for real-time, continuous monitoring through wearable respiratory sensors[9,73]. However, the performance of monometallic sensors can be effectively improved by the doping of other materials[74]. McConnell et al.[75] fabricated CNT-Pd composite sheets by electroplating pd on CNTs. The CNT-Pd composite sheet was assembled as a chemical sensor for H_2 detection, which has a low LOD and reversible response to H_2. The sensor was finally successfully integrated on a fabric material, showing its potential for wearable flexible sensor applications. Zhang et al.[44] presented reduced RGO decorated with silver nanoparticles (Ag NPs) as a sensing material for NH_3. Ag NPs enhanced the adsorption capacity of RGO for NH_3 electrons. The excellent performance of the sensor shows that it had the potential to serve applications in food safety, environment, and human health monitoring.

In addition, the doped material can be used as a reaction catalyst for the target gas to improve the sensing efficiency. The hollow structure obtained by the doping

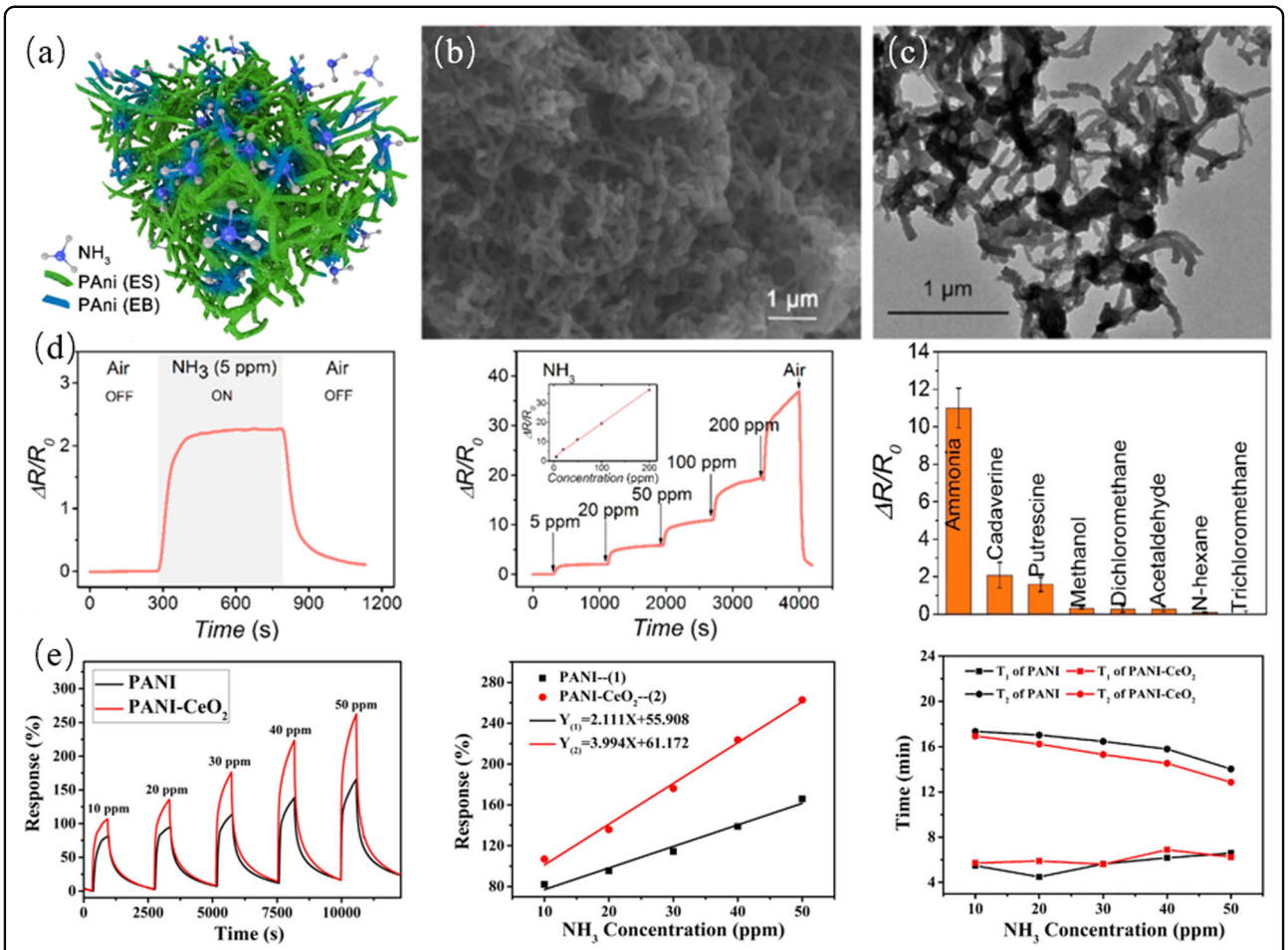

Fig. 8 Application of PANi in gas sensing. a The structure of PTS—PANi. **b** SEM image of PTS—PANi. **c** TEM image of PTS—PANi. **d** Sensing performances of PTS—PANi, response to 5 ppm NH_3, dynamic range, and selectivity. Reproduced with permission from ref. [63]. **e** Comparison of the sensing performance of pure PANi and PANi-CeO_2, response, dynamic range, and response/recovery time. Reproduced with permission from ref. [64]. Copyright Elsevier, 2018.

process has a larger specific surface area, which provides more adsorption sites for the gas to be measured and further improves the response and recovery characteristics of the sensor[76,77]. Shin et al.[78] prepared porous SnO_2 nanofibers consisting of pleated thin walls by electrostatic spinning and covered the fibers with Pt nanoparticles to make Pt-doped SnO_2 fibers, which exhibited excellent selectivity for toluene and acetone vapors. In comparison with undoped SnO_2 fibers, Pt-doped SnO_2 fibers exhibited a greater response to toluene as well as a faster response time and a low detection limit of 120 ppb for acetone vapor. The use of the special reaction mechanism of CuO with H_2S is also a typical application of doped materials as catalysts. Specifically, H_2S reacts with CuO nanoparticles and transforms them into CuS. The leftover hydrogen then "spills over" onto the surface of the host material and acts as a reducing agent, thus decreasing the resistance[7]. Shao et al.[79] fabricated CuO–SnO_2 by vapor-phase deposition and high-temperature oxidation. The reaction mechanism of CuO with H_2S, combined with the modulation effect of the p-n junction, leads to a significant improvement in the selectivity and sensitivity of the material to H_2S gas.

Improvements of the gas-sensitive properties of the SMO composites are mainly attributed to the respective compositions and the synergistic effect obtained by the heterojunction of the binary materials. In a p-n, p-p or n-n junction composed of two different semiconductors, electrons at high energies can be transferred across the oxide interface to unoccupied lower energy states to balance the Fermi energy level, leading to band bending. This energy transition can change the energy structure of the p-side and n-side, increasing the energy barrier and hence the resistance of the composite, and can therefore facilitate oxygen adsorption on the surface and achieve increased material sensitivity[7,80,81]. Yan et al.[82] synthesized α-Fe_2O_3/SnO_2 nanofibers with different doping concentrations by electrostatic spinning and compared

the sensitivity and operating conditions of the doped nanofibers with those of pure Fe_2O_3 nanofibers and pure SnO_2 nanofibers for ethanol. Experimental and theoretical studies have demonstrated that combining these two SMOs to form an n-n heterostructure is beneficial for enhancing the response and reducing the operating temperature. Wang et al.[83] successfully prepared electrostatically spun nanowebs with p-type NiO/n-type SnO_2 heterojunctions using an electrostatic spinning process, thermal compression and subsequent calcination process and then fabricated NiO/SnO_2 nanoweb sensors, which responded to 100 ppm ethanol by 1 order of magnitude higher than pure SnO_2 nanoweb sensors and exhibited better stability and response/recovery time. After decades of development, SMOs have been widely used as gas sensing materials. The main problems associated with using SMOs as sensing materials are their rigidity and the high temperature (100-500 °C) conditions needed to react them with gases, which not only leads to high energy consumption but also affects the long-term stability of the sensor performance, impeding the application of SMOs in wearable device applications. While doping SMOs with conductive polymers, utilizing the flexibility of the conductive polymer material and the heterojunction structure formed by SMO and the conductive polymer allows for the sensing performance of the composite to be effectively improved. Zhu et al.[84] synthesized PANi/Fe_2O_3 nanocomposites by a one-step hydrothermal method. At room temperature, the PANi/Fe_2O_3 nanocomposite thick film sensor has a good response to NH_3 gas, a low detection limit (0.3 ppm), good reproducibility and humidity resistance. Figure 9 demonstrates the electron microscope image of the hybrid nanomaterials, and Fig. 10 shows the sensing principle of the heterojunction.

Other materials

This section mainly includes various materials, such as TMDCs, metal-organic frameworks (MOFs) and paper. TMDCs and MOFs are new two-dimensional materials that have a high specific surface area, provide more active sites, and improve the physical adsorption and intermolecular interaction between the materials and the target gas. Moreover, relying on their porous nature, they can be easily functionalized with various sensing materials (metals and their derivatives, polymers, carbon quantum dots, etc.) to improve the sensing performance.

MOFs assembled from organic linkers and metal nodes have good chemical activity as well as highly ordered porous structures and have been of interest to many scholars since they were first discovered in the 1990s[85]. Various MOF thin film electronic devices can be fabricated by chemical vapor deposition (CVD)[86], substrate-seeded heteroepitaxy (SSH)[87], electrochemical fabrication (ECF)[88], liquid-phase epitaxy (LPE)[89], and Langmuir-Blodgett (LB)[90]. Based on the tunability of the pore size and surface groups of MOFs, it is possible to actively and passively filter and trap gases to enhance changes in the electronic conductivity of the composite due to the chemical reaction between MOFs and the target gas, which is expected to be a breakthrough strategy to achieve improved selectivity of gas sensors. Rui et al.[91] first prepared well-aligned plate-like multiwalled carbon nanotubes on Si/SiO_2 substrates by CVD, followed by controlled volume and drop-casting of different amounts of MOFs (e.g., ZIF-67-Co and MIL-88-Fe) into MWCNT plates, after which the coupled material was twisted into organic–inorganic fibers and finally annealed. The prepared MOF/MWCNT fibers have good electrical properties and exhibit good selectivity for NO_2, with a sensitivity as low as 0.1 ppm for NO_2 at room temperature.

TMDCs are composed of X-M-X with a sandwich laminate structure, where M is a transition metal element from group IV (Ti, Zr, Hf and so on), Group V (for instance V, Nb or Ta) or group VI (Mo, W and so on), and X is a chalcogen (S, Se or Te)[92]. The different layers are stacked together by van der Waals interactions and have strong in-plane bonding and weak out-of-plane interactions. Typical TMDCs that have been reported to be applied in gas sensors include WS_2, MoS_2, SnS_2, WSe_2, and $MoSe_2$[93]. TMDCs can be fabricated by a top-down approach (physical exfoliation, chemical exfoliation, ionic exfoliation, etc.) or bottom-up approach (CVD growth and epitaxial growth on SiC substrates, etc.)[92]. Due to its highly controllable number of layers and easily tunable surface properties, it has received much attention and applications. Yang et al.[94] developed a novel gas sensing platform based on porous LIG with a metal surface coating, which enables highly localized Joule heating (i.e., self-heating). Then, MoS_2/rGO was dispersed as a sensitive material in the LIG sensing region to result in an ultrasensitive chemiresistive NO_2 gas sensor, which has an actual detection limit of less than 1 ppb. With the advancement of research, ternary semiconducting alloys of TMDCs such as $Mo_xW_{1-x}S_2$[95], $Mo_xW_{1-x}Se_2$[96], and $WS_{2x}Se_{2-2x}$[97] have also been developed significantly. Ko et al.[98] revealed the decisive role of temperature in the conversion of WSe_2 to WS_2 by sulfidation and prepared $WS_{2x}Se_{2-2x}$ ($WS_{0.96}Se_{1.04}$, $WS_{0.66}Se_{1.34}$) alloy by precise temperature control. After that, WSe_2, WS_2, $WS_{0.96}$ $Se_{1.04}$, and $WS_{0.66}Se_{1.34}$ were used as sensitive materials to fabricate NO_2 flexible gas sensors. The sensing capability of the gas sensors of $WS_{0.66}Se_{1.34}$ and $WS_{0.96}Se_{1.04}$ alloys for NO_2 at room temperature was significantly improved, and the response to 500 ppm NO_2 exposure was ~ 1.6 and ~ 2.4 times higher than that of the WSe_2 gas sensor, respectively, which has potential for applications in advanced gas-sensing devices.

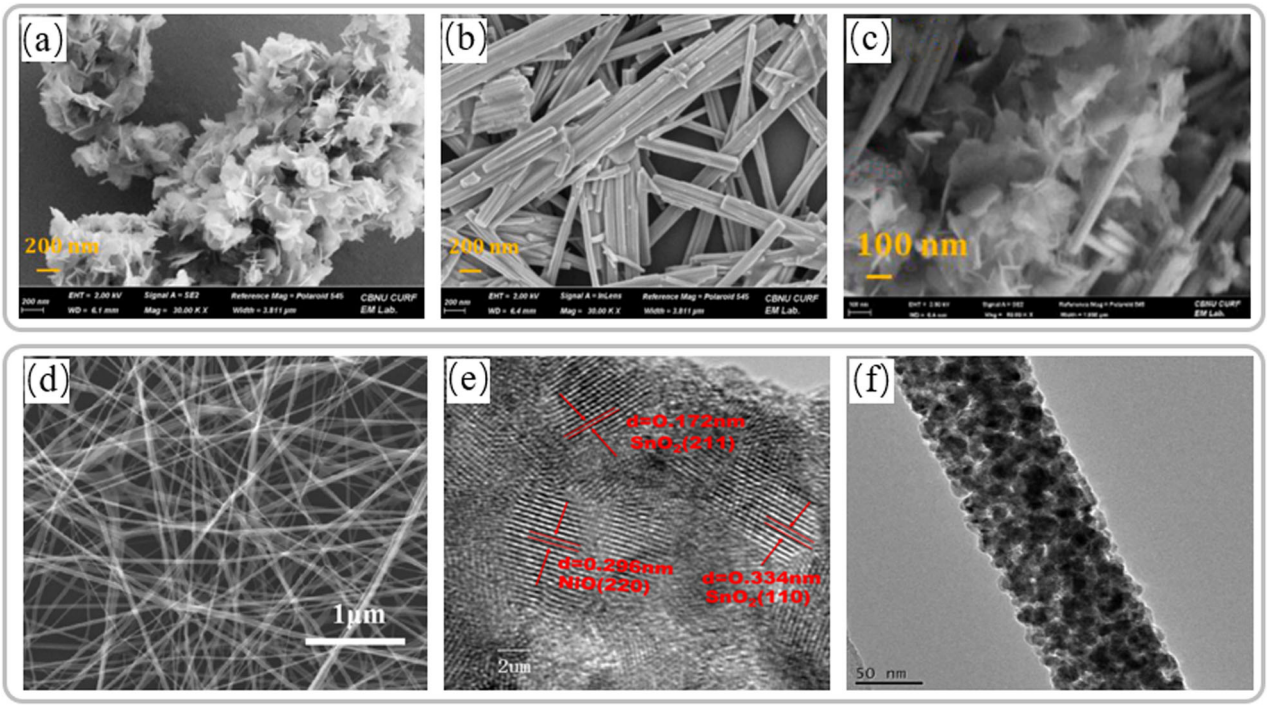

Fig. 9 Electron microscopy image of the hybrid nanomaterials. a FESEM image of NiO and **b** FESEM image of WO_3. (**c**) FESEM image of the NW3 sensor surface. Reproduced with permission from ref. [204]. Copyright Elsevier Sequoia, 2021. **d** SEM images of SnO_2/NiO nanowebs after calcination. **e** TEM image of the SnO_2/NiO nanofibers at high magnification. **f** At low magnification. Reproduced with permission from ref. [83]. Copyright Elsevier, 2016.

In recent years, cellulose paper has gradually appeared in flexible sensors (gas, humidity, strain, etc.) as a flexible, low-cost, lightweight, customizable, environmentally friendly, biodegradable, and renewable material[99]. Among the most impressive studies using paper as a sensing material for wearable devices is the study by F. Guder and Colleagues[100], who used the moisture absorption of the paper (at a relative humidity (RH) of 70%, the paper absorbs up to 10% of its weight in water) and the conductivity of paper that varies with different humidity levels to translate changes in humidity into changes in conductivity (Fig. 11d). Then, the humidity difference between the exhaled and inhaled gases during a respiratory cycle was measured to determine the respiration rate and respiration pattern. The full sensing part was manufactured only from common commercial paper, graphite and simple inkjet printing, and the sensor was usable without calibration or additional equipment. This platform provides a new development direction for wearable devices to be used to monitor information such as humidity and strain of the human body and the surrounding environment.

The paper-based sensors made by F. Guder were only used for the detection of some physical signals (humidity, stress). However, it is more important to detect biomarkers in exhaled gases, thus the additional processing steps are required during paper-based sensor fabrication. Compared with other substrates, due to the rough surface of paper, the electrodes on paper-based sensors can be prepared by simple and low-cost processing methods such as pencil drawing (conductive graphite) and conductive tape adhesion. In the recent years, paper-based sensors are already available for the detection of trace NH_3 gases[101] and NO_2 gases[102]. (Fig. 11)

Sensor evaluation factors

In the following discussion, we describe the performance of the wearable device by some characteristic parameters. Here, the meaning of each performance criterion in relation to the practical application of gas sensors is listed in this section as follows:

1. The "response" of a gas sensor represents the change in the measured electrical signal (e.g., I, C, R, or Z, V, or E) due to the introduction of an analyte. Typically, the gas response is usually defined as $R = (R_{air}\text{-}R_{gas})/R_{gas}$, where R_{air} is the resistance in the air and R_{gas} is the resistance in the target gas.
2. The "sensitivity" of the sensor is defined as the change in the sensor output response per unit concentration of analyte over the entire signal range, reflecting the

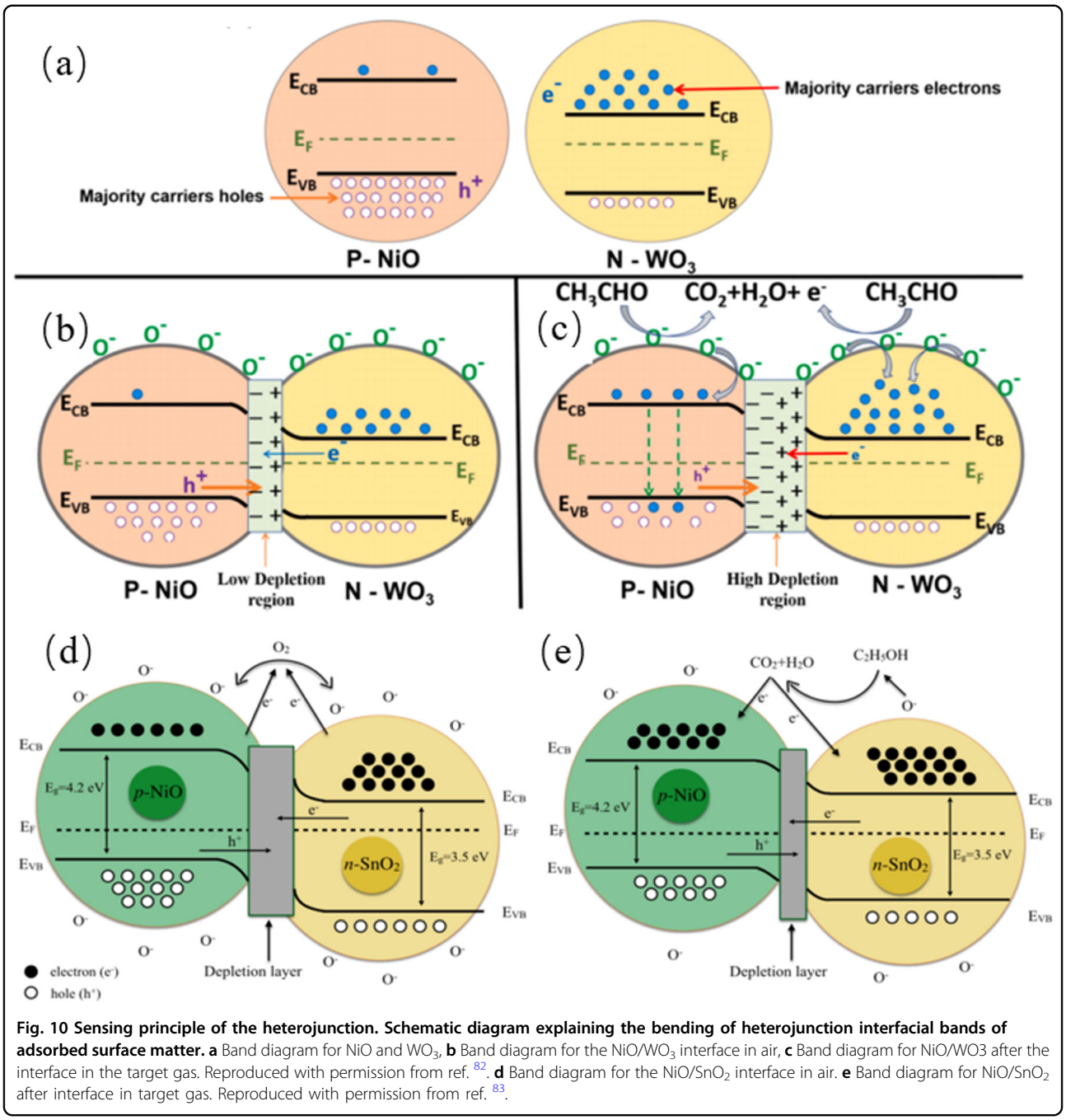

Fig. 10 Sensing principle of the heterojunction. Schematic diagram explaining the bending of heterojunction interfacial bands of adsorbed surface matter. a Band diagram for NiO and WO_3, **b** Band diagram for the NiO/WO_3 interface in air, **c** Band diagram for NiO/WO3 after the interface in the target gas. Reproduced with permission from ref. [82]. **d** Band diagram for the NiO/SnO_2 interface in air. **e** Band diagram for NiO/SnO_2 after interface in target gas. Reproduced with permission from ref. [83].

ability of the sensor to discriminate small differences in the concentration of the analyte gas.

3. The "limit of detection" (LOD) specifies the lowest gas concentration that the sensor can reliably detect. A low LOD is the basis for exhaled gas health monitoring.
4. The "resolution" of sensors is the smallest possible change that a sensor can perceive. Usually, the resolution of the sensor is not the same at each point in the full-scale range, so the maximum change in the input quantity that can cause a step change in the output in the full-scale range is often used as a resolution.
5. "Selectivity" is defined as the ability to distinguish target gas analytes in the presence of other gas analytes in the sample. The selectivity of wearable devices does not require us to detect and distinguish absolutely every substance in exhaled gas. For example, acetone, a marker of diabetes, is present in human exhaled gas at a concentration of ~1bbm.

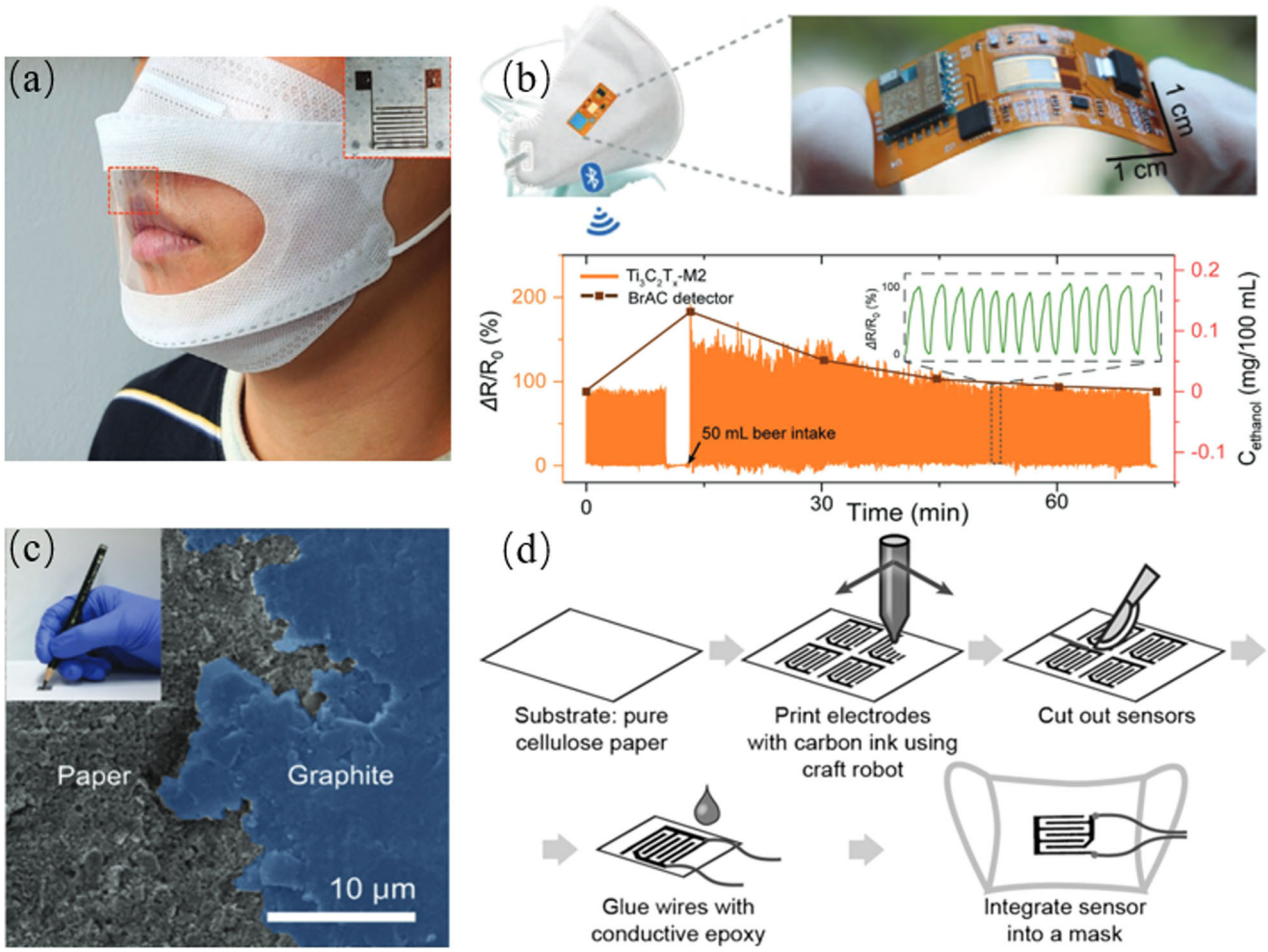

Fig. 11 Manufacturing and application examples of respiratory sensors. a Optical image of a face mask with integrated $Ni_3(HITP)_2$-based gas sensors. Reproduced with permission from ref. [284]. Copyright Wiley-VCH, 2022. **b** Flexible wireless VOC detection tags made with $Ti_3C_2T_x$-M_2 and real-time tracking of exhaled breath ethanol by the $Ti_3C_2T_x$-M_2 sensor with a commercial breath alcohol tester as a reference. Reproduced with permission from ref. [61]. **c** SEM image of the graphite (blue) on the paper. The inset shows a photograph of the writing process on the paper using an 8B pencil. Reproduced with permission from ref. [285]. Copyright John Wiley and Sons, 2017. **d** Schematic illustration of the fabrication of digitally printed paper sensors with graphite ink. Reproduced with permission from ref. [100].

In fact, there are approximately 3000 volatile substances in human exhaled gas, and most of the exhaled volatile gases are present at ppb/ppt concentrations. It is impractical to measure the cross-sensitivity between each substance and the target gas to achieve absolute selectivity. When judging the selectivity of the sensor for acetone, we only need to focus on substances with concentrations around ppm and do not need to pay too much attention to other gases.

6. "Response time" is the time needed for the sensor to reach a stable response, usually defined as the time to reach 90% of the final response, and "recovery time" is the opposite of the response time, being the time needed for the sensor to return to 90% of its original conductivity after the test gas has been released.
7. The "signal-to-noise ratio" (SNR) is the ratio of sensor signal power (desired) to background noise power (undesired).
8. The "dynamic range" (DR) of a sensor is defined as the span of its operation.

Respiratory sensors for health monitoring

As early as in ancient Greece, physicians discovered that the odor of human breath provided clues to certain diseases. The methods of detecting the concentration of various biomarkers in exhaled breath, as well as different breathing patterns, to determine a patient's illness and recovery have been proven and clinically applied in various medical fields[2,5], such as for the identification of several respiratory diseases, including asthma[103], chronic obstructive pulmonary disease (COPD)[104], pneumonia[105] and carbohydrate malabsorption[106]. The use of wearable

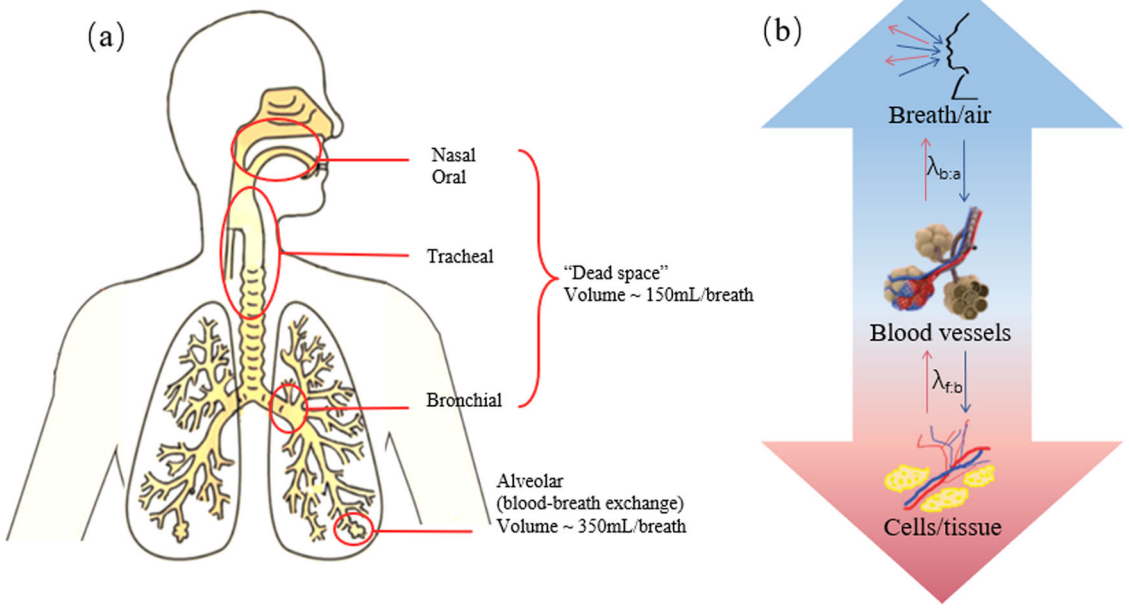

Fig. 12 Schematic illustrating the close physiological link between breath and blood. a Respiratory system and components of breath. **b** The simulation scheme that simulates the diffusion of VOC from the cells to the exhaled air. $\lambda_{f:b}$ – partition coefficient between fat and blood, and $\lambda_{b:a}$ – partition coefficient between blood and air. Reproduced with permission from ref. [286]. Copyright Royal Society of Chemistry, 2014.

respiratory sensors to collect data on the components of exhaled gas in real time and continuously to make judgments about the health status and provide warnings about the early onset of disease is in line with the trend of human-centered health care and the Internet of Everything. In this section, we will summarize the source and current status of detection of the major biomarkers in exhaled breath. Figure 12 illustrates the close physiological link between respiration and blood.

Exhaled gas detection

Volatile organic compounds

Exhaled gases contain thousands of compounds, including VOCs, volatile inorganic compounds, and nonvolatile substances. In terms of their origin, these substances may be produced by human metabolism or that of endomicrobiota (endogenous), or they may be absorbed from the environment and subsequently excreted after bodily circulation (exogenous). Inhaled air enters the alveoli of the lungs, and after metabolism, excretory products diffuse from the blood into the inhaled air and are eventually expelled as exhaled gas. Thus, exhaled air necessarily carries the fingerprints of endogenous metabolic processes[5]. Therefore, the monitoring of endogenous gas levels is of great interest for disease diagnosis and health monitoring.

VOCs are organic compounds with high vapor pressure at ordinary room temperature, and more than a thousand VOCs are found in human exhaled breath. Among them, common VOCs found in all humans include acetone, ethanol, methanol, isoprene, pentane and higher chain alcohols, aldehydes and ketones[107,108]. By detecting different concentrations of endogenous substances, it is possible to respond to different information in different parts of the patient. Additionally, exogenous VOCs detected in exhaled air are of interest, mainly because they are associated with personal exposure to carcinogens. Exogenous VOCs are often highly reactive and cause peroxidative damage to DNA, proteins and polyunsaturated fatty acids (PUFAs). The negative effects of these processes accumulate over the years and are thought to promote the chance of cancer[6]. To understand the potential of exhaled VOCs as markers of disease, it is important to understand their origin and their relationship to pathology. In this part of the review, respiratory biomarkers containing information on different diseases and metabolic disorders are discussed, their sources and generating factors are described, as well as sensing techniques for these specific gases in recent years.

Acetone Acetone can be used as a biological status marker for diabetes[109,110]. Patients with diabetes, either type I diabetes (where the body does not produce enough insulin) or type II diabetes (where the cells are insulin resistant), cannot rely on the decomposition of glucose for sufficient energy. In this case, fatty acids are broken down in the liver and replenish the body's energy needs, and the end products of the reaction, acetone and CO_2, are

excreted as waste products; hence, acetone is thus available as a good indicator of fat burning. As the diabetic patient's condition worsens, the patient's ability to decompose glucose further decreases, and ketogenesis increases, with a corresponding increase in acetone concentration in exhaled breath.

Acetone in the blood is exchanged and balanced with intra-alveolar air in the alveoli (exhaled gas contains approximately 1/330 times more acetone than plasma)[111]. By measuring the concentration of acetone in the exhaled breath, it is possible to determine the degree of diabetes (the acetone concentration in normal breath is ≤0.9 ppm, 0.9-1.8 ppm in moderate diabetic patients, and up to tens of ppm in severe diabetic patients) and the current physical state of the diabetic patient. Thus, acetone in exhaled breath may be a useful respiratory marker in patients with diabetes[112,113]. The measurement of acetone content in human exhaled gas also provides a range of information, such as diabetic ketoacidosis[114], physical exercise[115] and ketogenic diets[116].

Ethanol Ethanol is as the common "alcohol." The intestinal flora may be a potential source of trace amounts of endogenous ethanol, which in much smaller concentrations than exogenous ethanol[117]. Alcohol ingested through drinking is partially absorbed in the gastrointestinal tract and enters the bloodstream by diffusion. The concentration of acetone in breath is mainly governed by its concentration in the blood vessels of the upper respiratory tract and is therefore positively correlated with the amount of alcohol ingested. In healthy individuals who have not consumed alcohol, the concentration of ethanol in exhaled breath usually ranges from 13 to 1000 ppb, but up to several hundred ppm of ethanol can be detected in exhaled breath within eight hours after drinking alcohol[118]. Fuel cell-based portable breathalyzers have been widely used in traffic enforcement, health monitoring and safety incidents[118,119].

Isoprene The concentration of isoprene in the exhaled breath of normal healthy individuals is 12–580 ppb and is the main hydrocarbon produced endogenously in mammals, along with the cholesterol synthesis pathway, as a byproduct of cholesterol production and therefore has the same circadian rhythm as cholesterol[120,121]. Clinical studies have shown that isoprene can be used as a marker of cellular damage and cellular repair. Abnormal fluctuations in isoprene concentration can indicate lipid metabolism disorders and liver and lung fibrosis[108].

Alkanes The human body cannot produce methane on its own, and methane in the human body is mainly produced by anaerobic bacteria in the intestine (e.g., Methano brevibacter) by hydrogenating carbon dioxide. In general, methane is not present in human respiration, but it can also be found primarily in the feces if excessive methane is produced in the intestine and can be detected in human respiration[122,123]. Diseases caused by too much or too little methane in the human body include obesity[124], intestinal diseases[125], anorexia nervosa, etc.[5]. Pentane and ethane are the end products of cellular lipid peroxidation (LPO). Due to their low solubility in blood, these compounds are exhaled within a few lung passages, and the exhaled substances can then serve as markers of oxidative damage[103,126,127]. Finally, the levels of both pentane and ethane increase when subjected to mental[128] and physiological[129] stress.

Aldehyde There have been many reports showing that changes in the concentration of aldehydes in exhaled breath can be used as a biomarker for corresponding diseases. The current COVID-19 pandemic has created a need for inexpensive and rapid screening tools for this disease, of which respiratory biomarker screening may be a very promising way to discriminate, with studies indicating that acetaldehyde and acetone may be simultaneously increased in the breath of patients with COVID-19[130–132]. Shan et al.[132] fabricated exhaled gas sensing arrays using hybrid nanomaterials and made good test discriminations for both healthy and COVID-19 patients as well as for active disease and recovery by detecting biomarker concentrations of VOCs in exhaled gas. In addition, cancer patients tend to have an increase in endogenous enolenic aldehydes, hydroxyenolenic aldehydes and lipid peroxidation (LPO) di-aldol products[123]. As the concentration of these aldehydes increases in the blood and urine, it also increases in the exhaled breath. Therefore, aldehydes in exhaled breath can be used as biomarkers for a variety of diseases, especially lung cancer.

The above discussion show that human breath is a rich mixture of organic compounds that can be used as biomarkers for different diseases and metabolic disorders. In Table 1, we list different methods and detection performances developed in recent years for the detection of very low concentrations (ppmv, ppbv and pptv) of VOCs.

Volatile inorganic compounds

In addition to the main gaseous components (N_2, O_2, CO_2, noble gases and water vapor) and VOCs, exhaled gases contain various inorganic compounds, such as NO_2 (10–50 ppb), NO (1–20 ppb), NH_3 (0.5–2 ppm), CO (1–10 ppm), and H_2S (0–1.3 ppm). These abnormal changes in the concentration of exhaled substances may reflect internal problems caused by certain diseases.

Table 1 Gas sensors with potential for analysis of VOCs in exhaled gases.

Target gas	Sensing material	Synthesis method	Sensing performance	Ref.
Acetone	WO_3 NFs	electrospinning	LOD>1 ppm	15
	Si:WO_3	flame spray pyrolysis, anneal	DR: 4-70 ppm	183
	ZnO-PANI	self-assembly, coating	DR: 260−1300 ppm	184
	HAT7 and P3HT	Anneal, thermally deposited and oxygen-plasma etching	LOD >100ppb	185
	CS@rGO	chemical methods	LOD >20 ppb	186
	Pt/Al_2O_3 + Si/WO_3	flame spray pyrolysis, anneal	LOD>50 ppb	187
ethanol	Ti_3C_2Tx-M_2	Chemical substitution	DR: 20-500 ppm	61
	TiO_2@2D-TiC	Etch, single-stept hermalde composition	DR: 0.01−60 ppm	188
	PVA/MWCNTs	spray layer by layer	LOD >9.17 ppm	189
	WS_2/GONRs	chemical vapor transport, drop-casting method	DR: 1-21 ppm	38
	PVP-CB-EG	gravure printing, coating	LOD >40 ppm	190
	In_2O_3-PtNP NPs	oxygen reactive ion etching, etch and coat	LOD >3.9 ppb	191
	Bi_2WO_6/TiO_2	Electrospun, calcined	DR: 1-800 ppm	192
isoprene	Pt-doped SnO_2	flame spray pyrolysis, directly deposited and situ annealed	LOD>5 ppb	193
	rGO@ITO-PET	electrochemical-assisted deposition	LOD>237 ppb	194
	In_2O_3 NPs	co-precipitation method, anneal	LOD>1 ppb, R=143ppm-1	195
	Au-loaded ZnO	solvothermal method, Sputter and anneal	LOD>6ppb	196
	flower-like In_2O_3	hydrothermal method	LOD>5ppb	197
methane	PI/$SnSe_2$	Single source co-evaporation, polycondensation, imidization	LOD >0.02%	198
	PVP-CB-EG	gravure printing and coating	LOD >36 ppm	190
	Pt-doped SnO_2 nanoflowers	hydrothermal process, thermal reduction method	DR: 5-5000ppm	199
	Co-doped ZnO	sol-gel method, in situ growth	DR: 100-5000ppm	200
formaldehyde	ZnO/MXene NW	Etch, hydrothermal method	DR: 0.01-10 ppm, R=1.7128+1.0008X	201
	SnO_2/CMF	in situ growth	LOD>1 ppm	202
acetaldehyde	Ni-doped ZnO	chemical spray pyrolysis technique	LOD >10 ppm	203
	NiO+WO_3	hydrothermal chemical route, anneal	DR: 20-100ppm	204

Room temperature and air humidity if not specially marked.
P3HT poly(3-hexylthiophene), *HAT7* 2,3,6,7,10,11-hexakis(heptyloxy)triphenylene, *CS* chitosan, *CB* carbon black, *EG* ethylene glycol, *RH* relative humidity, *NFs* nanofibers, *NPs* nanoparticles, *NTs* nanotubes, *NW* nanowire, *NM* nanomembrane, *NRs* nanoribbons.

Ammonia (NH_3) NH_3 is used in the body to maintain blood acid–base balance and to produce nonessential amino acids. However, excess ammonia in the body can act as a toxin, and a healthy body will pass excess ammonia through the urea cycle to produce urea and ornithine, which are excreted from the body in the form of urine by the kidneys, and this cycle occurs in the liver and kidneys. If there is a problem with liver or kidney function, the excretion of ammonia through conversion to urea is limited, and some of the remaining ammonia will be excreted through respiration, as reflected by increased ammonia concentrations in exhaled air[133–135]. Therefore, abnormal concentrations of NH_3 in exhaled gas can provide early warning of some liver or kidney diseases, such as kidney failure[136], liver dysfunction[137], hepatic encephalopathy[138] and other diseases.

Nitrogen oxides Nitrogen oxides in exhaled gas mainly include NO_2 and NO. NO has an important physiological role in the regulation of vascular tone, response to vascular injury and hemostasis and acts as a neurotransmitter in cellular signal transduction (this work was later

Table 2 Gas sensors with potential for analysis of Inorganic compounds in exhaled gases.

Target gas	Sensing material	Synthesis method	Sensing performance	Ref.
NH_3	$CaCl_2$-infiltrated hydrogel	one-pot polymerization	LOD > 86 ppt	205
	PEDOT:PSS NW	soft lithography	LOD >100ppb	206
	CuBr	flame-aerosol deposition, brominated	90%RH, LOD>5 ppb, 5-5000 ppb	207
	graphene/MXenes	lasering	LOD >5 ppb	208
	ZnO/SnO_2	Electrospinning, hydrothermal method	LOD >10 ppm	209
	Ag-RGO	modified Hummers and Offman method, self-assembly	LOD >5 ppm	44
	PET-PANi-$CoFe_2O_4$	sol–gel combustion technique, In situ chemical oxidative polymerization	LOD >25 ppb, DR: 1-50 ppm	210
	PECOTEX	roll-to-roll coating	DR: 10-1000 ppm	211
	Ce-ZnO-X	spray method	DR: 0.1-10 ppm	212
	TiO_2/CNCs	Compound enzymatic hydrolysis, low-temperature liquid phase process	DR: 1.34-435 ppm	213
	PEDOT:PSS/IrOx/ hydrogel	chemical methods	DR: 17–7899 ppm	214
	Ti_3C_2T/RGO	wet-spinning, etch, modified Hummer's method	LOD >10 ppm	215
	CeO_2—CuBr	thermal evaporation, electron beam deposition	LOD >20 ppb	216
	NiO@CuO	chemical methods, electroless deposition	LOD >46.5 ppb	217
	BC/PANi-SSA/PAMPS	static fermentation, chemical methods	DR: 21.3-50 ppm	218
	SiO_2/PANI	sol-gel, electrospinning and calcination	LOD >400 ppb	219
	PANi/Fe_2O_3	Lyophilization, in situ deposited	LOD >0.3 ppm	84
	CA/PAM	one-pot polymerization method	LOD >3.5 ppb; R=8.4 ppm-1	220
NO_2	rGO-$ZnFe_2O_4$	soft lithography, e-beam and thermal evaporation	DR: 50 - 4000 ppb	221
	Pt_ZnO/ PRGO	chemical methods	LOD >0.1 ppm	222
	RGOH-(p)	single-step wet process	DR: 0.6-3 ppm	223
	rGO-ZnO NPs	atomic layer deposition, Electron beam-induced deposition	LOD >40	224
	ZnS NPs/N-rGO	modified Hummer's method, chemical methods	LOD >69 ppb	43
	g-C_3N_4/PANi	Electrospinning, doctor blade technique, situ polymerization	DR: 8–108 ppm	225
	$WS_{2x}Se_{2-2x}$	chemical methods	DR: 10-500 ppm	98
	MWCNT	Lasering, deposition	DR: 5-20 ppm	226
	TCNF/CNT	wet spinning	DR: 0.125-5 ppm	227
	TiO_2-spaced RGO	modified Hummer's method, minimally intensive layer delamination, layer-by-layer assembled	DR: 0.05-20ppm	228
	MoS_2-LIG	chemical methods, Laser, drop-casted	LOD >2 ppm	229
	rGO/SnO_2	Hummer's method, Spraying	DR: 20-100 ppm, R=0.0754+0.00182x(ppm)	45

Table 2 continued

Target gas	Sensing material	Synthesis method	Sensing performance	Ref.
	Borophene	In situ thermal decomposition method	LOD >200 ppb; DR: 0.2-100 ppm	230
	CNT/a-TiO_2	situ hydrolysis, calcination	LOD >500 ppb	231
	$Zn(OTf)_2$/PAM	assembled layer by layer	LOD >0.1 ppb	232
	SnO_2/MXene	self-assembly	LOD >0.03 ppb	233
	YSZ/SnO_2/SnS_2	self-sacrificial sulfidation method	DR: 0.02-4 ppm	234
NO	Cu-TCA/TiO_2	chemical bath deposition, chemical methods	LOD > 140 ppb; R=16.08+7.56X(ppm)	235
	LIG	laser	LOD >8.3 ppb, 4.18‰ppm−1	54
	LM@SnS_2	Sintering, Laser	LOD >1.32 ppb, 1092%/ppm	236
	DPPTT/Cu-BHT-NTs	self-assembly	LOD >5 ppb	237
	In_2O_3/ZnO	wet-chemical	LOD >100 ppm	238
H_2S	CuO-SWCNT	self-assembly	LOD >100 ppb	239
	Fe_2O_3-MPCNF	Electrospinning	DR: 0.2 - 100 ppm	240
	2D $NbWO_6$	chemical methods	150°C, LOD >0.5 ppm	241
	NO_2-UiO-66 NM	Electrospinning, spraying aqueous synthesis method	LOD >10 ppb; DR: 1-100 ppm	242
	PEDOT:PSS@Pd	Cross-linking, in-situ growth	DR: 0.25~6%	243
H_2	Pd/Si NM	Metal depositions	DR: 50−5000 ppm	244
	yarn@ Pd@Pt	sputter-deposition, spinning	LOD >1 ppm	245
	CNFs@Ni−Pt	electrospinning	LOD >100 ppm	246
	CNT-Pd	chemical vapor deposition, chemical methods	LOD > 0.1 mol %	75
	Pd NP	mask evaporation deposition	LOD >15 ppm	247
	Cs_2PtI_6	chemical methods	LOD >100 ppb	248
	rGO/SnO_2/PVDF	mortar pestle, E-beam evaporation	DR: 10-1000 ppm	249

*$Zn(OTf)_2$*Zn-zinc trifluoromethanesulfonate, *PAM* polyacrylamide, *PECOTEX* PEDOT:PSS-modified cotton conductive thread, *CNC* cellulose nanocrystals, *SSA* sulfosalicylic acid, *PAMPS* poly(2acrylamido-2-methyl-1-propane sulfonic acid), *YSZ* yttria-stabilized zirconia, *CA* carrageenan, *LM* liquid metal, *Cu-BHT* Cu-benzenehexathiol, *DPPTT* donor–acceptor copolymer semiconductor.

acknowledged with the Nobel Prize in Physiology or Medicine for the 'discoveries concerning nitric oxide as a signaling molecule in the cardiovascular system')[139]. Subsequently, it was shown that exhaled gas contains endogenous NO and is rapidly oxidized to NO_2 under natural environmental conditions. Exhaled nitric oxide is partially synthesized from the amino acid L-arginine by enzymes called NO synthases (NOS)[140], which are abundant in the lungs and may also be produced in the respiratory mucosa due to epithelial cell damage or inflammation[141]. Thus, changes in fractional exhaled nitric oxide (FeNO) may be indicative of a disease of the lungs or respiratory tract[142,143], e.g., asthma[144], chronic obstructive pulmonary disease (COPD)[145] and cystic fibrosis[146]. NO levels in the breath of healthy individuals are below 25 ppb, increase during exacerbations and decrease during recovery. A simple and absolutely noninvasive measurement of FeNO can be used as an additional diagnostic tool to screen patients suspected of having these diseases.

Hydrogen sulfide (H_2S) H_2S is a toxic gas with a 'rotten egg' smell and acts as a gas transmitter in humans and animals, participating in a variety of physical signaling processes, such as neuromodulation, cytoprotection, inflammation, apoptosis, and vascular tone regulation[147]. Hydrogen sulfide correlates with the severity of different respiratory diseases and airway inflammation and can be

used as a marker of airway inflammation and lower respiratory tract infections as well as the biological status of oral and dental health[148,149].

Hydrogen (H_2) The noninvasive hydrogen breath test (HBT) has been applied in clinical medicine to detect carbohydrate malabsorption[106]. In principle, when sugar in food is not absorbed in the small intestine and subsequently enters the colon, it becomes an energy supply for anaerobic colonic bacteria during fermentation, which releases CO_2, H_2 and CH_3. As it is produced by intestinal bacteria, intracolonic hydrogen diffuses through the colon wall into the systemic circulation and is carried to the lungs, where it is excreted from the body via exhaled breath. Therefore, HBT is commonly used to diagnose three physiological disorders: 1. Lactose intolerance: dietary sugars (e.g., lactose, galactose, etc.) are not properly digested[150]; 2. Small intestine bacterial overgrowth[151]; 3. Rapid passage of food through the small intestine. These scenarios can lead to a variety of symptoms, such as abdominal pain, bloating, flatulence and diarrhea[152] (Table 2).

Respiratory pattern monitoring

The four main vital signs routinely monitored by medical professionals are (i) body temperature, (ii) heart rate, (iii) respiration rate, and (iv) blood pressure[153]. The respiratory rate is a better indicator than other vital signs when differentiating between stable and unstable patients. Abnormalities in respiratory rate and pattern are important predictors of acute events or diseases, such as cardiac arrest, chronic obstructive pulmonary disease (COPD), pneumonia and asthma[154–156].

In clinical settings, uninterrupted respiratory monitoring is essential to improve the survival of patients with potential respiratory disease. For example, respiratory failure is one of the major symptoms of COVID-19 infection[157]. Respiratory arrest is one of the main symptoms of epilepsy (SUDEP)[158], brain injury[159], and heart failure[160] and is a cause of high mortality. Considering the nature of seizures, real-time respiratory monitoring can significantly improve survival in these diseases[161].

Healthy adults breathe approximately 12-20 times per minute and inhale or expel 6-8 L of gas per minute. Disturbances in the normal breathing patterns (i.e., breathing rate and depth) can reflect a person's underlying health status (i.e., stable or unstable). In a routine medical setting, specialized instruments can accurately measure a patient's breathing pattern by monitoring sound, airflow or chest motion; however, these processes include heavy instrumentation, expensive prices and high labor costs, which are not suitable for continuous monitoring of breathing patterns over long periods of time[5]. Therefore, there is a need to develop a low-cost, comfortable, easy-to-use, wearable respiratory sensor.

To obtain respiration-related parameters (frequency, flow rate, etc.), sensors can be placed near the mouth or nose and used to respond to differences in temperature and humidity of inhaled and exhaled gases within a respiratory cycle and to sensor pressure-bearing. Strain/pressure sensitive sensors can also be placed near the mouth and nose to sense the impact of airflow with each breath, or they can be affixed near the chest to respond to the expansion and contraction of the chest cavity. The corresponding respiratory cycle is reflected by periodic changes in the conductivity of the sensitive element.

The humidity in the exhaled gas is close to saturation, while the humidity of the inhaled gas depends on the environmental conditions in which the subject is exposed and generally differs significantly from the humidity of the exhaled gas. Therefore, based on the water absorption properties of sensing materials (mainly graphene, rGO, conductive polymers, MoS_2, CNTs, cellulose paper, etc.) and the changes in relevant parameters (conductance, capacitance, impedance, etc.) of the materials after water absorption, the fabrication of wearable humidity sensors on various flexible substrates provides a high-quality solution for the noninvasive and sustainable detection of respiratory frequency (Table 3).

EBC detection

Condensing and collecting exhaled breath is a noninvasive method for obtaining lung and airway samples and is a promising source of biomarkers for lung disease. In general, tidal breathing for 10 min can collect 1–3 mL of EBC from resting adult subjects, with the vast majority (>99%) of the EBC being condensed water vapor and the rest consisting of water-soluble volatiles or nonvolatile biological media[162]. Most of the VOCs and inorganic substances present in the exhaled gas are remixed into the EBC through condensation, and the content of each component in the EBC changes with the development of the disease and therapeutic interventions. Excitingly, the EBC contains not only those volatile substances in the exhaled gas but also a large number of nonvolatile solutes (e.g., hydrogen peroxide, isoprostane, nitrite, cytokines, and sodium ions)[163,164], which are not detectable in the gas phase[143].

The main source of nitrite in the respiratory tract is NO. In aqueous solutions, NO reacts rapidly with reactants to form more stable nitrogen oxides such as nitrite (NO^{-2}) and nitrate (NO^{-3}). Due to the relative stability of nitrite in EBC and the instability of NO in air (half-life of only a few seconds in the air), nitrite in EBC has promise as a biomarker of chronic respiratory inflammation[165]. Gholizadeh et al.[166] prepared nitrite electrochemical sensors on PDMS substrates by using screen-printed Au and

Table 3 Respiratory sensors for respiratory pattern detection pattern.

Objective	Sensing material	Synthesis method	Sensor performance	Ref.
RH	PU/ACNTs NFs	ultrasonication	5,11,16,20,29 with the RH of 11,33,59,75,95%	250
	ZnO/Ti/PTFE	hydrothermal method, layer by layer coating	1.8,13.9,28,44.8,85% with the RH of 50,60,70,80,90%	251
	LIG/ poly(ether-ether-ketone)	laser ablation, depositing, sputtering	R=1700kΩ/% RH	252
	SMPCF	Etch, self-assembly	Color changes with 0.02% RH	253
	Borophene–MoS_2	in situ van der Waals assembly	LOD>0.9736%RH, R= $(0.245X-0.549)^3$	254
	rGO/MoS_2	modified Hummer's method, ultrasonication	LOD>0.0109%RH, R=28.4RH-127.0	255
	Borophene–graphene	in situ thermal decomposition	Ln R=2.992ln (RH)-4.637	256
	rGO/PDAC	Layer by layer assembly	R=0.00143x + 0.975	257
	MoS_2/LIG	laser ablation	R=8% (0−50%RH), R=80%(50−100%RH)	258
Strain	rGO/CNTs	ultrasonic nanosoldering method	34.69@1%strain, R=1.21 kPa^{-1}	259
	MXene@spheres	wet-spinning, electrostatic assembly, spray-coating	R=174 (strain in 0-30%), 1187 (strain in 30-110%)	260
	PU/rGO/PDA/PFDT	Electrospinning, chemical methods	2,9,50 with the strain of 20,50,100, respectively	261
	GO/CNT	Self-assembly, freeze-drying method	R=0.15 (strain in 0-50%), 0.58 (strain in 50-80%)	262
	PANI-gelatin	sol-gel	R=1.4 (strain in 0-764.4%)	263
pressure	rGO/CNTs	ultrasonic nanosoldering method,	R=1.21 kPa^{-1}	259
	nano carbon	drop casting method	R=31.63 kPa^{-1} (0-2 kPa)	264
	TPU/CB	screen-printing	R=5.205 kPa^{-1} (0-2 kPa), 0.63 kPa^{-1} (>1200 kPa)	265
	PVDF/ZnO NFs	Electrospinning, magnetron sputtering	R=3.12 mV /kPa	266
	MXene/rGO	freeze-casting, annealing polymerization	R=0.28 kPa^{-1}(0-66.98 kPa)	267
	MXene ink-SF	dip-coating metho, screen-printing, etch	R=298.4kPa^{-1}(1.4-15.7 kPa) 171.9kPa^{-1}(15.7-39.3 kPa)	268
	CPDMS	Spraying, coating	R=124 kPa^{-1}(2−200 Pa), 0.39 kPa^{-1}(0.2−12 kPa), 0.02 kPa^{-1} (12−50 kPa)	269
	3D graphene	chemical vapor deposition	R=110 kPa^{-1}(0−0.2 Pa), 3kPa^{-1}(0.2−15 kPa), 0.26 kPa^{-1} (15−75 kPa)	25
	rGO/PC/W	Hydrothermal method, annealing	R=0.0122-0.41 kPa^{-1} (2-1200 kPa)	270
	a-PAN/G	Electrospinning, Annealing	R=44.5kPa^{-1}(0−1.2 kPa)	271
	MXene/Fe_3O_4/graphene	thermal chemical vapor deposition, coating, etching	R=4.71 kPa^{-1} (0-62.5 kPa)	272
	Laser-reduced graphene oxide	Lasering	R=0.95 kPa^{-1} (0-14 kPa)	273

SMPCF silk methylcellulose photonic crystal films, *PDAC* poly(diallyldimethylammonium chloride), *PDA* polydopamine, *PFDT* perfluorodecane-thiol, *CPDMS* carbon powder/polydimethylsiloxane, *PC* pillared carbon.

drop-in rGO as electrode materials, achieving detection limits as low as 830 nM for nitrite in EBC substrates with good linearity between 10 and 1000 μM concentrations. Seven precollected clinical EBC samples were subsequently tested using this sensing modality, which also showed good sensing performance. H_2O_2 measured in EBC has also been suggested as a respiratory marker of oxidative stress in lung disease. In the respiratory system, H_2O_2 may be released from both inflammatory and structural cells, including neutrophils, eosinophils, macrophages and epithelial cells[167]. H_2O_2 concentrations in EBC of healthy, nonsmoking young people ranged from 0 to 0.9 μmol/L[168]. Increased H_2O_2 concentrations in EBC were found in asthma[169], healthy smokers[170], COPD[171], and acute respiratory distress syndrome (ADRS)[172]. Chen et al.[173] prepared a disposable H_2O_2 electrochemical sensor using PEDOT:PSS-PB-EG-DVS as a sensitive material, which was titrated onto a gold working electrode. This chemical sensor had a low detection limit of 103 nM and showed good agreement with fluorometric results. In addition, the pH value of EBC depends on the volatilization and capture of airway acidic and alkaline source fluid, with a normal range between 7.4 and 8.8[168]. Although EBC pH is not equal to airway pH, it still allows for a qualitative noninvasive assessment of airway pH deviations[174].

It's difficult to predict the human disease status accurately through the detection of biomarkers in EBCs, mainly due to the lack of appropriate standards, interindividual variability, and the fact that many factors can influence the results of EBC collection. However, this lack of adoption does not detract from the potential of EBC analysis to address unmet medical needs and expand the portfolio of noninvasive testing for respiratory disease[168,175–178].

Challenges and prospects for wearable respiratory devices

Breathing provides direct biological information from the human body, and continuous health monitoring through breath analysis can be beneficial for health diagnosis and recovery monitoring. Analysis of exhaled gas composition and breathing patterns can replace traditional testing methods for noninvasive, easy-to-use and continuous health monitoring but comes with multiple challenges.

The challenges of wearable respiratory sensors

Existing sensing materials applied to detect exhaled gases still require development in order to find use in practical applications go. Using SMO or MOFs as the sensing layer material, the sensors usually need to work at high temperature, under which the oxygen ions on the surface of the SMO will react with the water vapor in the air to form reactive hydroxyl groups (OH^-) prior to the gas-sensing reaction, which significantly changes the resistance of the sensor and deteriorates its response to the exhaled gas. The contact of graphene and conductive polymers with the detected gases is mostly through van der Waals forces, resulting in weak selectivity and sensitivity of these sensing materials. In addition, when composite materials are applied, the SNR of the sensor may also be reduced due to the weak bonding between the various materials. Finally, the low LOD, high selectivity and sensitivity of the sensors usually come at the cost of irreversibility of the interaction between the detection gas and the sensing material, which may result in long recovery times and memory effects[179].

A variety of factors influence respiratory monitoring: the rate and volume during exhalation, the choice of mouth or nose breathing method, and the individual's internal conditions (age, diet, gender, physiologic status and possibly genetic background), which can all influence the proportion of various biomarkers in the exhaled breath[142,180,181]. Moreover, the sources of biomarkers in exhaled breath are complex, and the various markers collected may be inhaled from the air and then exhaled, produced autonomously by the human body or metabolized by nonhumans (microorganisms, bacteria, etc.). For daily health monitoring, we are only interested in markers produced during human biological activity, but it is difficult to distinguish the origin of these markers and to eliminate their interference in breath collection and analysis[103,182].

The prospects of wearable respiratory sensors

With the in-depth research and application of various novel sensing materials, the detection of low concentrations of target gases at room temperature with low power consumption has become possible, establishing a foundation for the application of respiratory wearable devices. Composites based on conductive polymers offer the advantages of favorable mechanical robustness, low sensing temperatures, simple fabrication, and suitability for large-scale industrial production. Combining materials such as SMO and C-based materials with conductive polymers to create e-textiles with clothes and masks is one of the directions for the development of room temperature gas sensing devices. In addition, most respiratory sensors currently monitor respiratory rate and intensity by measuring humidity and strain. A promising application of flexible gas sensors is the analysis of exhaled gases to diagnose diseases such as asthma, pneumonia, and influenza; therefore, more attention should be given to this application. Finally, EBC contains a large number of biomarkers, some of which are not even detectable in exhaled gas; there is great potential to leverage the presence of these biomarkers in various application. However, research on EBC is scarce and immature, and more relevant research and standardization

are needed. Combined with detection techniques such as interstitial fluid and sweat, we expect that rapid advances in this field will be realized in the future.

Acknowledgements
This project is supported by the Chongqing Natural Science Foundation (CSTB2022NSCQ-MSX1085), State Key Laboratory of Electrical Insulation and Power Equipment (EIPE22206), Guangxi Key Laboratory of Automatic Detecting Technology and Instruments (YQ22208), Interdisciplinary Training Program for Young Teachers and Students (No. 415010300081), and Science and Technology Project of Jilin Provincial Education Department (JJKH20230811KJ, JJKH20241267KJ).

Author details
[1]School of Mechanical and Aerospace Engineering, Jilin University, Changchun 130025, China. [2]State Key Laboratory of Electrical Insulation and Power Equipment, Xi'an Jiaotong University, Xi'an 710049, China. [3]Guangxi Key Laboratory of Automatic Detecting Technology and Instruments, Guilin University of Electronic Technology, Guilin 541004, China. [4]School of Mechanical and Electrical Engineering, Changchun University of Science and Technology, Changchun 130022, China. [5]Chongqing Research Institute, Jilin University, Chongqing 401122, China

Author contributions
X.Y. and Z.Y. conceived the theme and directed the project. Y.Y. collected the literature and wrote the manuscript. C.H., J.L. and B.Q. prepared the figures. Z.Y. and Y.Y. reviewed and edited the manuscript. All the authors have read and approved the final manuscript.

Conflict of interest
The authors declare no competing interests.

Received: 1 December 2022 Revised: 16 September 2023 Accepted: 27 October 2023
Published online: 09 February 2024

References

1. Wang, C., Yin, L., Zhang, L., Xiang, D. & Gao, R. Metal oxide gas sensors: sensitivity and influencing factors. *Sensors* **10**, 2088–2106 (2010).
2. Phillips, M. Breath tests in medicine. *Sci. Am.* **267**, 74–9 (1992). 1992.
3. Phillips, M. et al. Variation in volatile organic compounds in the breath of normal humans. *J. Chromatogr. B* **729**, 75–88 (1999).
4. Fenske, J. D. & Paulson, S. E. Human breath emissions of VOCs. *J. Air Waste Manag. Assoc.* **49**, 594–598 (1999).
5. Mathew, T. L., Pownraj, P., Abdulla, S. & Pullithadathil, B. Technologies for clinical diagnosis using expired human breath analysis. *Diagnostics (Basel, Switzerland)* **5**, 27–60 (2015).
6. Righettoni, M., Amann, A. & Pratsinis, S. E. Breath analysis by nanostructured metal oxides as chemo-resistive gas sensors. *Materials Today* **18**, 163–171 (2015).
7. Zhou, X. R. et al. Ordered porous metal oxide semiconductors for gas sensing. *Chin. Chem. Lett.* **29**, 405–416 (2018).
8. Barsan, N. & Weimar, U. Conduction model of metal oxide gas sensors. *J. Electroceramics* **7**, 143–167 (2001).
9. Alrammouz, R., Podlecki, J., Abboud, P., Sorli, B. & Habchi, R. A review on flexible gas sensors: from materials to devices. *Sens. Actuators A Phys.* **284**, 209–231 (2018).
10. Alsyouri, H. M. & Lin, J. Y. S. Gas diffusion and microstructural properties of ordered mesoporous silica fibers. *J. Phys. Chem. B* **109**, 13623–13629 (2005).
11. Jin, C. Q. et al. Influence of nanoparticle size on ethanol gas sensing performance of mesoporous alpha-Fe(2)O3 hollow spheres. *Mater. Sci. Eng. B Adv. Funct. Solid-State Mater.* **224**, 158–162 (2017).
12. Rout, C. S., Hegde, M. & Rao, C. N. R. H2S sensors based on tungsten oxide nanostructures. *Sens. Actuators B Chem.* **128**, 488–493 (2008).
13. Wagner, T., Haffer, S., Weinberger, C., Klaus, D. & Tiemann, M. Mesoporous materials as gas sensors. *Chem. Soc. Rev.* **42**, 4036–4053 (2013). 2013.
14. Jang, J. S., Choi, S. J., Kim, S. J., Hakim, M. & Kim, I. D. Rational design of highly porous SnO2 nanotubes functionalized with biomimetic nanocatalysts for direct observation of simulated diabetes. *Adv. Funct. Mater.* **26**, 4740–4748 (2016).
15. Xu, H. et al. Mesoporous WO3 nanofibers with crystalline framework for high-performance acetone sensing. *Front. Chem.* **7**, 266 (2019).
16. Yoon, J.-W. et al. Trimodally porous SnO2 nanospheres with three-dimensional interconnectivity and size tunability: a one-pot synthetic route and potential application as an extremely sensitive ethanol detector. *NPG Asia Mater.* **8**, e244 (2016).
17. Yang, Y. et al. A laser-engraved wearable sensor for sensitive detection of uric acid and tyrosine in sweat. *Nat. Biotechnol.* **38**, 217 (2020).
18. Kong, J. et al. Nanotube molecular wires as chemical sensors. *Science* **287**, 622–625 (2000).
19. Agarwal, P. B. et al. Flexible NO2 gas sensor based on single-walled carbon nanotubes on polytetrafluoroethylene substrates. *Flex. Print. Electron.* **3**, 035001 (2018).
20. Gao, Z. et al. Fiber gas sensor-integrated smart face mask for room-temperature distinguishing of target gases. *Nano Res.* **11**, 511–519 (2018).
21. Robinson, J. A., Snow, E. S., Badescu, S. C., Reinecke, T. L. & Perkins, F. K. Role of defects in single-walled carbon nanotube chemical sensors. *Nano Lett.* **6**, 1747–1751 (2006).
22. Zhao, J. J., Buldum, A., Han, J. & Lu, J. P. Gas molecule adsorption in carbon nanotubes and nanotube bundles. *Nanotechnology* **13**, 195–200 (2002). Pii s0957-4484(02)30254-x.
23. Guo, S. Y., Hou, P. X., Zhang, F., Liu, C. & Cheng, H. M. Gas Sensors Based on Single-Wall Carbon Nanotubes. *Molecules* **27**, 5381 (2022).
24. Novoselov, K. S. et al. Electric field effect in atomically thin carbon films. *Science* **306**, 666–669 (2004).
25. Xia, K. L., Wang, C. Y., Jian, M. Q., Wang, Q. & Zhang, Y. Y. CVD growth of fingerprint-like patterned 3D graphene film for an ultrasensitive pressure sensor. *Nano Res.* **11**, 1124–1134 (2018).
26. Qiu, X. Y., Bouchiat, V., Colombet, D. & Ayela, F. Liquid-phase exfoliation of graphite into graphene nanosheets in a hydrocavitating 'lab-on-a-chip. *Rsc Adv.* **9**, 3232–3238 (2019).
27. Dresselhaus, M. S. & Dresselhaus, G. Intercalation compounds of graphite. *Adv. Phys.* **51**, 1–186 (2002).
28. Riedl, C., Coletti, C. & Starke, U. Structural and electronic properties of epitaxial graphene on SiC(0 0 0 1): a review of growth, characterization, transfer doping and hydrogen intercalation. *J. Phys. D Appl. Phys.* **43**, 374009 (2010).
29. Kim, K. S. et al. Atomic layer etching of graphene through controlled ion beam for graphene-based electronics. *Sci. Rep.* **7**, 2462 (2017).
30. Singh, S. U. et al. Advanced wearable biosensors for the detection of body fluids and exhaled breath by graphene. *Microchim. Acta* **189**, 236 (2022).
31. Bolotin, K. I. et al. Ultrahigh electron mobility in suspended graphene. *Solid State Commun.* **146**, 351–355 (2008).
32. Singh, E., Meyyappan, M. & Nalwa, H. S. FlexiblE GRAPHENE-BASED WEARABLE GAS AND CHEMICAL SEnsors. *ACS Appl. Mater. Interfaces* **9**, 34544–34586 (2017).
33. Ma, J. et al. Gas sensor based on defective graphene/pristine graphene hybrid towards high sensitivity detection of NO2. *AIP Adv.* **9**, 075207 (2019).
34. Kim, Y. H. et al. Self-activated transparent all-graphene gas sensor with endurance to humidity and mechanical bending. *ACS Nano* **9**, 10453–10460 (2015).
35. Marcano, D. C. et al. Improved synthesis of graphene oxide. *ACS Nano* **4**, 4806–4814 (2010).
36. Sun, L. & Fugetsu, B. Mass production of graphene oxide from expanded graphite. *Mater. Lett.* **109**, 207–210 (2013).
37. Li, N., Chen, X. D., Chen, X. P., Ding, X. & Li, X. Y. Subsecond response of humidity sensor based on graphene oxide quantum dots. *IEEE Electron Device Lett.* **36**, 615–617 (2015).
38. Ahmadvand, H., Zad, A. I., Mohammadpour, R., Hosseini-Shokouh, S. H. & Asadian, E. Room temperature and high response ethanol sensor based on two dimensional hybrid nanostructures of WS2/GONRs. *Sci. Rep.* **10**, 14799 (2020).

39. Duy, L. T. et al. Flexible transparent reduced graphene oxide sensor coupled with organic dye molecules for rapid dual-mode ammonia gas detection. *Adv. Functional Mater.* **26**, 4329–4338 (2016).
40. Gao, X. F., Jang, J. & Nagase, S. Hydrazine and thermal reduction of graphene oxide: reaction mechanisms, product structures, and reaction design. *J. Phys. Chem. C* **114**, 832–842 (2010).
41. Wang, G. X. et al. Facile synthesis and characterization of graphene nanosheets. *J. Phys. Chem. C* **112**, 8192–8195 (2008).
42. Pei, S. F. & Cheng, H. M. The reduction of graphene oxide. *Carbon* **50**, 3210–3228 (2012).
43. Chen, X. W. et al. Wearable NO2 sensing and wireless application based on ZnS nanoparticles/nitrogen-doped reduced graphene oxide. *Sens. Actuators B Chem.* **345**, 130423 (2021).
44. Zhang, L. et al. Highly sensitive NH3 wireless sensor based on Ag-RGO composite operated at room-temperature. *Sci. Rep.* **9**, 9942 (2019).
45. Zhang, F. Z. et al. A flexible and wearable NO2 gas detection and early warning device based on a spraying process and an interdigital electrode at room temperature. *Microsyst. Nanoeng.* **8**, 40 (2022).
46. Lin, J. et al., Laser-induced porous graphene films from commercial polymers. *Nat. Commun.* 5, https://doi.org/10.1038/ncomms6714. (2014).
47. Parmeggiani, M. et al. PDMS/polyimide composite as an elastomeric substrate for multifunctional laser-induced graphene electrodes. *ACS Appl. Mater. Interfaces* **11**, 33221–33230 (2019).
48. You, R. et al. Laser fabrication of graphene-based flexible electronics. *Adv. Mater.* **32**, 1901981 (2020).
49. Dimiev, A. M. et al. Direct real-time monitoring of stage transitions in graphite intercalation compounds. *ACS Nano* **7**, 2773–2780 (2013).
50. Biswas, R. K., Vijayaraghavan, R. K., McNally, P., O'Connor, G. M. & Scully, P. Graphene growth kinetics for CO2 laser carbonization of polyimide. *Mater. Lett.* **307**, 131097 (2022).
51. Li, G. J., Mo, X. Y., Law, W. C. & Chan, K. C. Wearable fluid capture devices for electrochemical sensing of sweat. *ACS Appl. Mater. Interfaces* **11**, 238–243 (2019).
52. Abdulhafez, M., Tomaraei, G. N. & Bedewy, M. Fluence-dependent morphological transitions in laser-induced graphene electrodes on polyimide substrates for flexible devices. *ACS Appl. Nano Mater.* **4**, 2973–2986 (2021).
53. Muzyka, K. & Xu, G. Laser-induced graphene in facts, numbers, and notes in view of electroanalytical applications: a review. *Electroanalysis* **34**, 574–589 (2022).
54. Yang, L. et al. Moisture-resistant, stretchable NOx gas sensors based on laser-induced graphene for environmental monitoring and breath analysis. *Microsyst. Nanoeng.* **8**, 78 (2022).
55. Chyan, Y. et al. Laser-induced graphene by multiple lasing: toward electronics on cloth, paper, and food. *ACS Nano* **12**, 2176–2183 (2018).
56. Naguib, M. et al. Two-dimensional nanocrystals produced by exfoliation of Ti3AlC2. *Adv. Mater.* **23**, 4248–4253 (2011).
57. Xin, M., Li, J. A., Ma, Z., Pan, L. J. & Shi, Y. MXenes and their applications in wearable sensors. *Front. Chem.* **8**, 297 (2020).
58. Naguib, M., Mochalin, V. N., Barsoum, M. W. & Gogotsi, Y. 25th anniversary article: MXenes: a new family of two-dimensional materials. *Adv. Mater.* **26**, 992–1005 (2014).
59. Pei, Y. Y. et al. Ti3C2TX MXene for sensing applications: recent progress, design principles, and future perspectives. *ACS Nano* **15**, 3996–4017 (2021).
60. Reddy, M. S. B., Kailasa, S., Marupalli, B. C. G., Aich, S. & Sadasivuni, K. K. A family of 2D-MXenes: synthesis, properties, and gas sensing applications. *ACS Sensors* **7**, 2132–2163 (2022).
61. Li, X. et al. Room temperature VOCs sensing with termination-modified Ti3C2Tx MXene for wearable exhaled breath monitoring. *Adv. Mater. Technol.* **7**, 2100872 (2022).
62. Xing, H. et al. MXene/MWCNT electronic fabric with enhanced mechanical robustness on humidity sensing for real-time respiration monitoring. *Sens. Actuators B Chem.* **361**, 131704 (2022).
63. Ma, Z. et al. Highly sensitive, printable nanostructured conductive polymer wireless sensor for food spoilage detection. *Nano Lett.* **18**, 4570–4575 (2018).
64. Liu, C. H. et al. A high-performance flexible gas sensor based on self-assembled PANI-CeO2 nanocomposite thin film for trace-level NH3 detection at room temperature. *Sens. Actuators B Chem.* **261**, 587–597 (2018).
65. Li, S. et al. Flexible ammonia sensor based on PEDOT:PSS/silver nanowire composite film for meat freshness monitoring. *IEEE Electron Device Lett.* **38**, 975–978 (2017).
66. Khan, I. & Saeed, K. Nanoparticles: properties, applications and toxicities. *Arabian J. Chem.* **12**, 908–931 (2019).
67. Koga, K. Electronic and catalytic effects of single-atom pd additives on the hydrogen sensing properties of Co3O4 nanoparticle films. *ACS Appl. Mater. Interfaces* **12**, 20806–20823 (2020).
68. Rai, P., Kim, Y. S., Song, H. M., Song, M. K. & Yu, Y. T. The role of gold catalyst on the sensing behavior of ZnO nanorods for CO and NO2 gases. *Sens. Actuators B Chem.* **165**, 133–142 (2012).
69. Marikutsa, A., Novikova, A., Rumyantseva, M., Khmelevsky, N. & Gaskov, A. Comparison of Au-functionalized semiconductor metal oxides in sensitivity to VOC. *Sens. Actuators B Chem.* **326**, 128980 (2021).
70. D'Arienzo, M. et al. One-step preparation of SnO2 and Pt-doped SnO2 as inverse opal thin films for gas sensing. *Chem. Mater.* **22**, 4083–4089 (2010).
71. Kolmakov, A., Klenov, D. O., Lilach, Y., Stemmer, S. & Moskovits, M. Enhanced gas sensing by individual SnO2 nanowires and nanobelts functionalized with Pd catalyst particles. *Nano Lett.* **5**, 667–673 (2005).
72. Kim, W., Jang, B., Lee, H.-S. & Lee, W. Reliability and selectivity of H-2 sensors composed of Pd Film nanogaps on an elastomeric substrate. *Sens. Actuators B Chem.* **224**, 547–551 (2016).
73. Wang, M. & Feng, Y. Palladium-silver thin film for hydrogen sensing. *Sens. Actuators B Chem.* **123**, 101–106 (2007).
74. Wolfe, D. B., Love, J. C., Paul, K. E., Chabinyc, M. L. & Whitesides, G. M. Fabrication of palladium-based microelectronic devices by microcontact printing. *Appl. Phys. Lett.* **80**, 2222–2224 (2002).
75. McConnell, C. et al. Hydrogen sensors based on flexible carbon nanotube-palladium composite sheets integrated with ripstop fabric. *ACS Omega* **5**, 487–497 (2020).
76. Xu, X. W., Wang, J. & Long, Y. C. Zeolite-based materials for gas sensors. *Sensors* **6**, 1751–1764 (2006).
77. Della Gaspera, E. et al. Colloidal approach to Au-loaded TiO2 thin films with optimized optical sensing properties. *J. Mater. Chem.* **21**, 4293–4300, (2011). 2011.
78. Shin, J. et al. Thin-wall assembled SnO2 fibers functionalized by catalytic Pt nanoparticles and their superior exhaled-breath-sensing properties for the diagnosis of diabetes. *Adv. Funct. Mater.* **23**, 2357–2367 (2013).
79. Shao, F. et al. Heterostructured p-CuO (nanoparticle)/n-SnO2 (nanowire) devices for selective H2S detection. *Sens. Actuators B Chem.* **181**, 130–135 (2013).
80. Miller, D. R., Akbar, S. A. & Morris, P. A. Nanoscale metal oxide-based heterojunctions for gas sensing: a review. *Sens.s Actuators B Chem.* **204**, 250–272 (2014).
81. Wang, Z., Tian, Z., Han, D. & Gu, F. Highly sensitive and selective ethanol sensor fabricated with In-doped 3DOM ZnO. *ACS Appl. Mater. Interfaces* **8**, 5466–5474 (2016).
82. Yan, S., Xue, J. Z. & Wu, Q. S. Synchronous synthesis and sensing performance of alpha-Fe2O3/SnO2 nanofiber heterostructures for conductometric C2H5OH detection. *Sens. Actuators B Chem.* **275**, 322–331 (2018).
83. Wang, Y., Zhang, H. & Sun, X. H. Electrospun nanowebs of NiO/SnO2 p-n heterojunctions for enhanced gas sensing. *Appl. Surface Sci.* **389**, 514–520 (2016).
84. Zhu, C. H. et al. One step synthesis of PANI/Fe2O3 nanocomposites and flexible film for enhanced NH3 sensing performance at room temperature. *Nanotechnology* **30**, 255502 (2019).
85. Zhang, L.-T., Zhou, Y. & Han, S.-T. The role of metal-organic frameworks in electronic sensors. *Angew. Chem. Int. Ed.* **60**, 15192–15212 (2021).
86. Stassin, T. et al. Vapour-phase deposition of oriented copper dicarboxylate metal-organic framework thin films. *Chem. Commun.* **55**, 10056–10059 (2019).
87. Falcaro, P. et al. Centimetre-scale micropore alignment in oriented polycrystalline metal-organic framework films via heteroepitaxial growth. *Nat. Mater.* **16**, 342 (2017).
88. Alizadeh, S. & Nematollahi, D. Electrochemically assisted self-assembly technique for the fabrication of mesoporous metal-organic framework thin films: composition of 3D hexagonally packed crystals with 2D honeycomb-like mesopores. *J. Am. Chem. Soc.* **139**, 4753–4761 (2017).
89. Ikigaki, K. et al. MOF-on-MOF: oriented growth of multiple layered thin films of metal-organic frameworks. *Angew. Chem. Int. Ed.* **58**, 6886–6890 (2019).
90. Rubio-Gimenez, V. et al. High-quality metal-organic framework ultrathin films for electronically active interfaces. *J. Am. Chem. Soc.* **138**, 2576–2584 (2016).

91. Rui, K. et al. Dual-function metal-organic framework-based wearable fibers for gas probing and energy storage. *ACS Appl. Mater. Interfaces* **10**, 2837–2842 (2018).
92. Wang, Q. H., Kalantar-Zadeh, K., Kis, A., Coleman, J. N. & Strano, M. S. Electronics and optoelectronics of two-dimensional transition metal dichalcogenides. *Nat. Nanotechnol.* **7**, 699–712 (2012).
93. Zhou, T. T. & Zhang, T. Recent progress of nanostructured sensing materials from 0D to 3D: overview of structure-property-application relationship for gas sensors. *Small Methods* **5**, 2100515 (2021).
94. Yang, L. et al. Novel gas sensing platform based on a stretchable laser-induced graphene pattern with self-heating capabilities. *J. Mater. Chem. A* **8**, 6487–6500 (2020).
95. Tan, C. L. et al. Preparation of single-layer MoS2xSe2(1-x) and MoxW1-xS2 nanosheets with high-concentration metallic 1T phase. *Small* **12**, 1866–1874 (2016).
96. Sun, Y. F. et al. Low-temperature solution synthesis of transition metal dichalcogenide alloys with tunable optical properties. *J. Am. Chem. Soc.* **139**, 11096–11105 (2017).
97. Duan, X. et al. Synthesis of WS2xSe2-2x alloy nanosheets with composition-tunable electronic properties. *Nano Lett.* **16**, 264–269 (2016).
98. Ko, K. Y. et al. High-performance gas sensor using a large-area WS2xSe2-2x alloy for low-power operation wearable applications. *ACS Appl. Mater. Interfaces* **10**, 34163–34171 (2018).
99. Nassar, J. M. et al. Paper skin multisensory platform for simultaneous environmental monitoring. *Adv. Mater. Technol.* **1**, 1600004 (2016).
100. Guder, F. et al. Paper-based electrical respiration sensor. *Angew. Chem. Int. Ed.* **55**, 5727–5732 (2016).
101. Barandun, G. et al. Cellulose fibers enable near-zero-cost electrical sensing of water-soluble gases. *ACS Sens.* **4**, 1662–1669 (2019).
102. Zhang, J. et al. Pencil-trace on printed silver interdigitated electrodes for paper-based NO2 gas sensors. *Appl. Phys. Lett.* **106**, 143101 (2015).
103. Rufo, J. C., Madureira, J., Fernandes, E. O. & Moreira, A. Volatile organic compounds in asthma diagnosis: a systematic review and meta-analysis. *Allergy* **71**, 175–188 (2016).
104. Bos, L. D., Sterk, P. J. & Fowler, S. J. Breathomics in the setting of asthma and chronic obstructive pulmonary disease. *J. Allergy Clin. Immunol.* **138**, 970–976 (2016).
105. van Oort, P. M. et al. The potential role of exhaled breath analysis in the diagnostic process of pneumonia-a systematic review. *J. Breath Res.* **12**, 024001 (2018).
106. Ruzsanyi, V. et al. Diagnosing lactose malabsorption in children: difficulties in interpreting hydrogen breath test results. *J. Breath Res.* **10**, 016015 (2016).
107. Jalal, A. H. et al. Prospects and challenges of volatile organic compound sensors in human healthcare. *ACS Sens.* **3**, 1246–1263 (2018).
108. Mehaney, A., Alrowaili, Z. A., Elsayed, H. A., Taha, T. A. & Ahmed, A. M. Theoretical investigations of Tamm plasmon resonance for monitoring of isoprene traces in the exhaled breath: Towards chronic liver fibrosis disease biomarkers. *Phys. Lett. A* **413**, 127610 (2021).
109. Smith, D., Spanel, P., Fryer, A. A., Hanna, F. & Ferns, G. A. A. Can volatile compounds in exhaled breath be used to monitor control in diabetes mellitus? *J. Breath Res.* **5**, 022001 (2011).
110. Buszewski, B., Kesy, M., Ligor, T. & Amann, A. Human exhaled air analytics: Biomarkers of diseases. *Biomed. Chromatogr.* **21**, 553–566 (2007).
111. Crofford, O. B. et al. Acetone in breath and blood. *Trans. Am. Clin. Climatolog. Assoc.* **88**, 128–139 (1977).
112. Henderson, M. J., Karger, B. A. & Wren Shall, G. A. Acetone in the breath; a study of acetone exhalation in diabetic and nondiabetic human subjects. *Diabetes* **1**, 188 (1952).
113. Sulway, M. J. & Malins, J. M. Acetone in diabetic ketoacidosis. *Lancet* **2**, 736–740 (1970).
114. Ruzsanyi, V. & Kalapos, M. P. Breath acetone as a potential marker in clinical practice. *J. Breath Res.* **11**, 024002 (2017).
115. Koeslag, J. H. Post-exercise ketosis and the hormone response to exercise: a review. *Med. Sci. Sports Exerc.* **14**, 327–334 (1982). 1982. [Online]. Available: <Go to ISI>://MEDLINE:6759842.
116. Musa-Veloso, K. et al. Breath acetone predicts plasma ketone bodies in children with epilepsy on a ketogenic diet. *Nutrition* **22**, 1–8 (2006).
117. Cope, K., Risby, T. & Diehl, A. M. Increased gastrointestinal ethanol production in obese mice: Implications for fatty liver disease pathogenesis. *Gastroenterology* **119**, 1340–1347 (2000).
118. Umasankar, Y. et al., "Wearable alcohol monitoring device with auto-calibration ability for high chemical specificity," in *13th IEEE International Conference on Wearable and Implantable Body Sensor Networks (BSN)*, San Francisco, CA, 2016 Jun 14-17 2016, in International Conference on Wearable and Implantable Body Sensor Networks, 353–358. (IEEE Xplore, 2016)
119. Polissar, N. L., Suwanvijit, W. & Gullberg, R. G. The accuracy of handheld pre-arrest breath test instruments as a predictor of the evidential breath alcohol test results. *J. Forensic Sci.* **60**, 482–487 (2015).
120. Cailleux, A. & Allain, P. Isoprene and sleep. *Life sciences* **44**, 1877–80, (1989). 1989.
121. Mochalski, P., King, J., Mayhew, C. A. & Unterkofler, K. A review on isoprene in human breath. *J. Breath Res.* **17**, 037101 (2023).
122. Levitt, M. D., Furne, J. K., Kuskowski, M. & Ruddy, J. Stability of human methanogenic flora over 35 years and a review of insights obtained from breath methane measurements. *Clin. Gastroenterol. Hepatol.* **4**, 123–129 (2006).
123. Das, S. & Pal, M. Review-non-invasive monitoring of human health by exhaled breath analysis: a comprehensive review. *J. Electrochem. Soc.* **167**, 037562 (2020).
124. Haines, A. P., Imeson, J. D. & Wiggins, H. S. Relation of breath methane with obesity and other factors. *Int. J. Obes.* **8**, 675–680 (1984).
125. Wilder-Smith, C. H., Olesen, S. S., Materna, A. & Drewes, A. M. Breath methane concentrations and markers of obesity in patients with functional gastrointestinal disorders. *United Eur. Gastroenterol. J.* **6**, 595–603 (2018).
126. Riely, C. A., Cohen, G. & Lieberman, M. Ethane evolution: a new index of lipid peroxidation. *Science (New York, N.Y.)* **183**, 208–10 (1974). 1974.
127. Allerheiligen, S. R., Ludden, T. M. & Burk, R. F. The pharmacokinetics of pentane, a by-product of lipid peroxidation. *Drug Metab. Dispos. Biolog. Fate Chem.* **15**, 794–800 (1987).
128. Ivanova, S. M., Orlov, O. N., Brantova, S. S., Labetskaia, O. I. & Davydova, N. A. Effect of intensive operator activity on lipid peroxidation processes in the human body. *Kosmicheskaia Biologiia I Aviakosmicheskaia Meditsina* **20**, 20–22 (1986).
129. Leaf, D. A., Kleinman, M. T., Hamilton, M. & Barstow, T. J. The effect of exercise intensity on lipid peroxidation. *Med. Sci. Sports Exerc.* **29**, 1036–9 (1997). 1997.
130. Torok, Z. M. et al. Breath biomarkers as disease indicators: sensing techniques approach for detecting breath gas and COVID-19. *Chemosensors* **10**, 167 (2022).
131. Chen, H. et al. COVID-19 screening using breath-borne volatile organic compounds. *J. Breath Res.* **15**, 4 (2021). 047104.
132. Shan, B. et al. Multiplexed nanomaterial-based sensor array for detection of COVID-19 in exhaled breath. *Acs Nano* **14**, 12125–12132 (2020).
133. Burton, B. K. Urea cycle disorders. *Clin. Liver Dis.* **4**, 815–30, (2000). vi2000.
134. Mew, N. A., Yudkoff, M. & Tuchman, M. Stable isotopes in the diagnosis and treatment of inherited hyperammonemia. *J. Pediatr. Biochem.* **4**, 57–63 (2014).
135. Walker, V. Ammonia toxicity and its prevention in inherited defects of the urea cycle. *Diabetes Obesity Metab.* **11**, 823–835 (2009).
136. Davies, S., Spanel, P. & Smith, D. Quantitative analysis of ammonia on the breath of patients in end-stage renal failure. *Kidney Int.* **52**, 223–8 (1997).
137. Agarwal, A., Rai, S. K., Lin, Y. C., Patnaik, R. K. & Yeh, J. A. Ammonia selectivity over acetone by viscosity modulation of silicone oil filter for diagnosing liver dysfunction. *Ecs J. Solid State Sci. Technol.* **9**, 115030 (2020).
138. He, Y. et al. Partial pressure of NH3 in cirrhotic patients with and without hepatic encephalopathy. *J. Gastrointest. Liver Dis.* **20**, 169–174 (2011).
139. Pham, Y. L. & Beauchamp, J. Breath biomarkers in diagnostic applications. *Molecules* **26**, 5514 (2021).
140. Palmer, R. M. The L-arginine: nitric oxide pathway. *Curr. Opin. Nephrol. Hypertens.* **2**, 122–8, (1993).
141. Saleh, D., Ernst, P., Lim, S., Barnes, P. J. & Giaid, A. Increased formation of the potent oxidant peroxynitrite in the airways of asthmatic patients is associated with induction of nitric oxide synthase: effect of inhaled glucocorticoid. *FASEB J.* **12**, 929–37 (1998).
142. Ashutosh, K. Nitric oxide and asthma: a review. *Curr. Opin. Pulm. Med.* **6**, 21–5 (2000).
143. Cao, W. Q. & Duan, Y. X. Breath analysis: Potential for clinical diagnosis and exposure assessment. *Clin. Chem.* **52**, 800–811 (2006).
144. Kharitonov, S. A., Yates, D. & Barnes, P. J. Increased nitric oxide in exhaled air of normal human subjects with upper respiratory tract infections. *Euro. Respir. J.* **8**, 295–7 (1995).
145. Barnes, P. J. & Kharitonov, S. A. Exhaled nitric oxide: a new lung function test. *Thorax* **51**, 233–7 (1996).

146. Dotsch, J. et al. Airway nitric oxide in asthmatic children and patients with cystic fibrosis. *Euro. Respir. J.* **9**, 2537–40 (1996).
147. Olas, B. Hydrogen sulfide in signaling pathways. *Clin. Chim. Acta* **439**, 212–218 (2015).
148. Tangerman, A. & Winkel, E. G. Intra- and extra-oral halitosis: finding of a new form of extra-oral blood-borne halitosis caused by dimethyl sulphide. *J. Clin. Periodontol.* **34**, 748–755 (2007).
149. Morselli-Labate, A. M., Fantini, L. & Pezzilli, R. Hydrogen sulfide, nitric oxide and a molecular mass 66 u substance in the exhaled breath of chronic pancreatitis patients. *Pancreatology* **7**, 497–504 (2007).
150. Robles, L. & Priefer, R. Lactose intolerance: what your breath can tell you. *Diagnostics* **10**, 412 (2020).
151. Bauer, T. M. et al. Diagnosis of small intestinal bacterial overgrowth in patients with cirrhosis of the liver: poor performance of the glucose breath hydrogen test. *J. Hepatol.* **33**, 382–386 (2000).
152. Shin, W. Medical applications of breath hydrogen measurements. *Anal. Bioanal. Chem.* **406**, 3931–3939 (2014).
153. Evans, D., Hodgkinson, B. & Berry, J. Vital signs in hospital patients: a systematic review. *Int. J. Nursing Stud.* **38**, 643–650 (2001).
154. Tai, H. L., Wang, S., Duan, Z. H. & Jiang, Y. D. Evolution of breath analysis based on humidity and gas sensors: potential and challenges. *Sens. Actuators B Chem.* **318**, 128104 (2020).
155. Khan, Y., Ostfeld, A. E., Lochner, C. M., Pierre, A. & Arias, A. C. Monitoring of vital signs with flexible and wearable medical devices. *Adv. Mater.* **28**, 4373–4395 (2016).
156. Guo, L., Berglin, L., Wiklund, U. & Mattila, H. Design of a garment-based sensing system for breathing monitoring. *Textile Res. J.* **83**, 499–509 (2013).
157. Zaim, S., Chong, J. H., Sankaranarayanan, V. & Harky, A. COVID-19 and multiorgan response. *Curr. Problems Cardiol.* **45**, 100618 (2020).
158. Ryvlin, P. et al. Incidence and mechanisms of cardiorespiratory arrests in epilepsy monitoring units (MORTEMUS): a retrospective study. *Lancet Neurol.* **12**, 966–977 (2013).
159. Greer, D. M. Mechanisms of injury in hypoxic-ischemic encephalopathy: Implications to therapy. *Semin. Neurol.* **26**, 373–379 (2006).
160. Alviar, C. L. et al. Positive pressure ventilation in the cardiac intensive care unit. *J. Am. Coll. Cardiol.* **72**, 1532–1553 (2018).
161. Mojoli, F., Bouhemad, B., Mongodi, S. & Lichtenstein, D. Lung ultrasound for critically Ill patients. *Am. J. Respir. Crit. Care Med.* **199**, 701–714 (2019).
162. Effros, R. M. et al. Dilution of respiratory solutes in exhaled condensates. *Am. J. Respir. Crit. Care Med.* **165**, 663–669 (2002).
163. Miekisch, W., Schubert, J. K. & Noeldge-Schomburg, G. F. E. Diagnostic potential of breath analysis - focus on volatile organic compounds. *Clin. Chim. Acta* **347**, 25–39 (2004).
164. Zacharasiewicz, A. et al. Repeatability of sodium and chloride in exhaled breath condensates. *Pediatric Pulmonol.* **37**, 273–275 (2004).
165. Baraldi, E. et al. Safety and success of exhaled breath condensate collection in asthma. *Archives Dis. Childhood* **88**, 358–360 (2003).
166. Gholizadeh, A. et al. Toward point-of-care management of chronic respiratory conditions: electrochemical sensing of nitrite content in exhaled breath condensate using reduced graphene oxide. *Microsyst. Nanoeng.* **3**, 17022 (2017).
167. Wewel, A. R. et al. Time course of exhaled hydrogen peroxide and nitric oxide during chemotherapy. *Eur. Respir. J.* **27**, 1033–1039 (2006).
168. Horvath, I. et al., Exhaled breath condensate: methodological recommendations and unresolved questions. *Euro. Respir. J.* **26**, 523–548, (2005).
169. Jobsis, Q., Raatgeep, H. C., Hermans, P. W. & de Jongste, J. C. Hydrogen peroxide in exhaled air is increased in stable asthmatic children. *Euro. Respir. J.* **10**, 519–521 (1997).
170. Nowak, D. et al. Increased content of hydrogen peroxide in the expired breath of cigarette smokers. *Euro. Respir. J.* **9**, 652–7 (1996). 1996.
171. De Benedetto, F. et al. Validation of a new technique to assess exhaled hydrogen peroxide: results from normals and COPD patients. *Monaldi Archives Chest Disease = Archivio Monaldi Malattie Del Torace* **55**, 185–188 (2000).
172. Heard, S. O. et al. The influence of liposome-encapsulated prostaglandin E-1 on hydrogen peroxide concentrations in the exhaled breath of patients with the acute respiratory distress syndrome. *Anesth. Analg.* **89**, 353–357 (1999).
173. Chen, Y. C. & O'Hare, D. Exhaled breath condensate based breath analyser - a disposable hydrogen peroxide sensor and smart analyser. *Analyst* **145**, 3549–3556 (2020).
174. Davis, M. D., Montpetit, A. & Hunt, J. Exhaled breath condensate an overview. *Immunol. Allergy Clin. N. Am.* **32**, 363 (2012).
175. Davis, M. D. & Montpetit, A. J. Exhaled breath condensate an update. *Immunol. Allergy Clin. N. Am.* **38**, 667 (2018).
176. Sawano, M., Takeshita, K., Ohno, H. & Oka, H. RT-PCR diagnosis of COVID-19 from exhaled breath condensate: a clinical study. *J. Breath Res.* **15**, 037103 (2021).
177. Cepelak, I. & Dodig, S. Exhaled breath condensate: a new method for lung disease diagnosis. *Clin. Chem. Lab. Med.* **45**, 945–952 (2007).
178. Scheideler, L., Manke, H. G., Schwulera, U., Inacker, O. & Hammerle, H. Detection of nonvolatile macromolecules in breath. A possible diagnostic tool? *Am. Rev. Respir. Dis.* **148**, 778–84 (1993). 1993.
179. Konvalina, G. & Haick, H. Sensors for breath testing: from nanomaterials to comprehensive disease detection. *Acc. Chem. Res.* **47**, 66–76 (2014).
180. Shirasu, M. & Touhara, K. The scent of disease: volatile organic compounds of the human body related to disease and disorder. *J. Biochem.* **150**, 257–266 (2011).
181. Costello, B. D. et al. A review of the volatiles from the healthy human body. *J. Breath Res.* **8**, 014001 (2014).
182. Fowler, S. J. Breath analysis for label-free characterisation of airways disease. *Eur. Respir. J.* **51**, 1702586 (2018).
183. Guntner, A. T. et al. Guiding ketogenic diet with breath acetone sensors. *Sensors* **18**, 3655 (2018).
184. Davis, D. et al. Flexible paper-based room-temperature acetone sensors with ultrafast regeneration. *ACS Appl. Mater. Interfaces* **15**, 25734–25743 (2023).
185. Chuang, M. Y. et al. Room-temperature-operated organic-based acetone gas sensor for breath analysis. *Sens. Actuators B Chem.* **260**, 593–600 (2018).
186. Wang, L. L., Jackman, J. A., Park, J. H., Tan, E. L. & Cho, N. J. A flexible, ultrasensitive chemical sensor with 3D biomimetic templating for diabetes-related acetone detection. *J. Mater. Chem. B* **5**, 4019–4024 (2017).
187. Weber, I. C., Braun, H. P., Krumeich, F., Guntner, A. T. & Pratsinis, S. E. Superior acetone selectivity in gas mixtures by catalyst-filtered chemoresistive sensors. *Adv. Sci.* **7**, 2001503 (2020).
188. Raghu, A. V., Karuppanan, K. K., Nampoothiri, J. & Pullithadathil, B. Wearable, flexible ethanol gas sensor based on TiO2 nanoparticles-grafted 2D-titanium carbide nanosheets. *ACS Appl. Nano Mater.* **2**, 1152–1163 (2019).
189. Maity, D., Rajavel, K. & Kumar, R. T. R. Polyvinyl alcohol wrapped multiwall carbon nanotube (MWCNTs) network on fabrics for wearable room temperature ethanol sensor. *Sens. Actuators B Chemical* **261**, 297–306 (2018).
190. Wei, H. L., Kumar, P. & Yao, D. J. Printed resistive sensor array combined with a flexible substrate for ethanol and methane detection. *ECS J. Solid State Sci. Technol.* **9**, 115008 (2020).
191. Kim, S. Y. et al. Alcohol gas sensors capable of wireless detection using In2O3/Pt nanoparticles and Ag nanowires. *Sens. Actuators B Chem.* **259**, 825–832 (2018).
192. Wang, K., Wei, W., Lou, Z., Zhang, H. & Wang, L. L. 1D/2D heterostructure nanofiber flexible sensing device with efficient gas detectivity. *Appl. Surface Sci.* **479**, 209–215 (2019).
193. van den Broek, J., Guntner, A. T. & Pratsinis, S. E. Highly selective and rapid breath isoprene sensing enabled by activated alumina filter. *ACS Sensors* **3**, 677 (2018).
194. Chen, Q. F., Liu, D., Lin, L. M. & Wu, J. M. Bridging interdigitated electrodes by electrochemical-assisted deposition of graphene oxide for constructing flexible gas sensor. *Sens. Actuators B Chem.* **286**, 591–599 (2019).
195. Zheng, Q., Lee, J. H., Kim, S. J., Lee, H. S. & Lee, W. Excellent isoprene-sensing performance of In2O3 nanoparticles for breath analyzer applications. *Sens.s Actuators B Chem.* **327**, 128892 (2021).
196. Saito, N., Haneda, H., Watanabe, K., Shimanoe, K. & Sakaguchi, I. Highly sensitive isoprene gas sensor using Au-loaded pyramid-shaped ZnO particles. *Sens. Actuators B Chem.* **326**, 128999 (2021).
197. Han, B. Q. et al. Hydrothermal synthesis of flower-like In2O3 as a chemiresistive isoprene sensor for breath analysis. *Sens. Actuators B Chem.* **309**, 127788 (2020).
198. Chen, M. et al. Large-scale synthesis of single-crystalline self-standing SnSe2 nanoplate arrays for wearable gas sensors. *Nanotechnology* **29**, 455501 (2018).
199. Xue, D. P., Wang, P. T., Zhang, Z. Y. & Wang, Y. Enhanced methane sensing property of flower-like SnO2 doped by Pt nanoparticles: A combined experimental and first-principle study. *Sens. Actuators B Chem.* **296**, 126710 (2019).

200. Niu, F. et al. Synthesizing metal oxide semiconductors on doped Si/SiO2 flexible fiber substrates for wearable gas sensing. *Research* **6**, 0100 (2023).
201. Zhang, D. Z., Mi, Q., Wang, D. Y. & Li, T. T. MXene/Co3O4 composite based formaldehyde sensor driven by ZnO/MXene nanowire arrays piezoelectric nanogenerator. *Sens. Actuators B Chem.* **339**, 129923 (2021).
202. Li, Y. X. et al. Rational design and in situ growth of SnO2/CMF composites: insightful understanding of the formaldehyde gas sensing mechanism and enhanced gas sensing properties. *J. Mater. Chem. C* **8**, 12418–12426 (2020).
203. Mani, G. K. & Rayappan, J. B. B. ZnO nanoarchitectures: Ultrahigh sensitive room temperature acetaldehyde sensor. *Sens. Actuators B Chem.* **223**, 343–351 (2016).
204. Nakate, U. T., Yu, Y. T. & Park, S. High performance acetaldehyde gas sensor based on p-n heterojunction interface of NiO nanosheets and WO3 nanorods. *Sens. Actuators B Chem.* **344**, 130264 (2021).
205. Wu, Z. X. et al. Ion-conductive hydrogel-based stretchable, self-healing, and transparent NO2 sensor with high sensitivity and selectivity at room temperature. *Small* **17**, 2104997 (2021).
206. Tang, N. et al. A fully integrated wireless flexible ammonia sensor fabricated by soft nano-lithography. *ACS Sens.* **4**, 726–732 (2019).
207. Guntner, A. T., Wied, M., Pineau, N. J. & Pratsinis, S. E. Rapid and selective NH3 sensing by porous CuBr. *Adv. Sci.* **7**, 1903390 (2020).
208. Zhang, C. et al. Laser processing of crumpled porous graphene/mxene nanocomposites for a standalone gas sensing system. *Nano Lett.* **23**, 3435–3443 (2023).
209. Yang, T. et al. Wearable smart yarn sensor based on ZnO/SnO2 heterojunction for ammonia detecting. *J. Mater. Sci.* **57**, 21946–21959 (2022).
210. Alharthy, R. D. & Saleh, A. A novel trace-level ammonia gas sensing based on flexible PAni-CoFe2O4 nanocomposite film at room temperature. *Polymers* **13**, 3077 (2021).
211. Alshabouna, F. et al. PEDOT:PSS-modified cotton conductive thread for mass manufacturing of textile-based electrical wearable sensors by computerized embroidery. *Mater. Today* **59**, 56–67 (2022).
212. Wang, S. et al. An integrated flexible self-powered wearable respiration sensor. *Nano Energy* **63**, 103829 (2019).
213. Tong, X., Zhang, X. J., Li, J. & Wang, H. Flexible NH3 gas sensor based on TiO2/cellulose nanocrystals composite film at room temperature. *J. Mater. Sci. Mater. Electron.* **32**, 23566–23577 (2021).
214. Serafini, M. et al. A wearable electrochemical gas sensor for ammonia detection. *Sensors* **21**, 7905 (2021).
215. Lee, S. H. et al. Room-temperature, highly durable Ti3C2Tx MXene/graphene hybrid fibers for NH3 gas sensing. *ACS Appl. Mater. Interfaces* **12**, 10434–10442 (2020).
216. Li, H. Y., Lee, C. S., Kim, D. H. & Lee, J. H. Flexible room-temperature NH3 sensor for ultrasensitive, selective, and humidity-independent gas detection. *ACS Appl. Mater. Interfaces* **10**, 27858–27867 (2018).
217. Zhou, Y. L., Wang, J. & Li, X. K. Flexible room-temperature gas sensor based on poly (para-phenylene terephthalamide) fibers substrate coupled with composite NiO@CuO sensing materials for ammonia detection. *Ceramics Int.* **46**, 13827–13834 (2020).
218. Yang, L. Y. et al. Wearable and flexible bacterial cellulose/polyaniline ammonia sensor based on a synergistic doping strategy. *Sens. Actuators B Chem.* **334**, 129647 (2021).
219. Nie, Q. X. et al. Facile fabrication of flexible SiO2/PANI nanofibers for ammonia gas sensing at room temperature. *Colloids Surfaces a Physicochem. Eng. Aspects* **537**, 532–539 (2018).
220. Wu, J. et al. Stretchable, stable, and room-temperature gas sensors based on self-healing and transparent organohydrogels. *ACS Appl. Mater. Interfaces* **12**, 52070–52081 (2020).
221. Bag, A. et al. A room-temperature operable and stretchable NO2 gas sensor composed of reduced graphene oxide anchored with MOF-derived ZnFe2O4 hollow octahedron. *Sens. Actuators B Chem.* **346**, 130463 (2021).
222. Kang, J. Y. et al. 2D layer assembly of Pt-ZnO nanoparticles on reduced graphene oxide for flexible NO2 sensors. *Sens. Actuators B-Chem.* **331**, 129371 (2021).
223. Duy, L. T. & Seo, H. Eco-friendly, self-healing, and stretchable graphene hydrogels functionalized with diol oligomer for wearable sensing applications. *Sens. Actuators B Chem.* **321**, 128507 (2020).
224. Moon, D. B. et al. A stretchable, room-temperature operable, chemiresistive gas sensor using nanohybrids of reduced graphene oxide and zinc oxide nanorods. *Sens. Actuators B Chem.* **345**, 130373 (2021).
225. Khalifa, M. & Anandhan, S. Highly sensitive and wearable NO2 gas sensor based on PVDF nanofabric containing embedded polyaniline/g-C3N4 nanosheet composites. *Nanotechnology* **32**, 485504 (2021).
226. Park, J., Ryu, C., Jang, I., Jung, S. I. & Kim, H. J. A study of strain effect on stretchable carbon nanotube gas sensors. *Mater. Today Commun.* **33**, 105007 (2022).
227. Cho, S. Y. et al. Continuous meter-scale synthesis of weavable tunicate cellulose/carbon nanotube fibers for high-performance wearable sensors. *ACS Nano* **13**, 9332–9341 (2019).
228. Song, Y. Y. et al. MXene-Derived TiO2 nanoparticles intercalating between RGO nanosheets: an assembly for highly sensitive gas detection. *ACS Appl. Mater. Interfaces* **13**, 39772–39780 (2021).
229. Yan, W. H. et al. Size-tunable flowerlike MoS2 nanospheres combined with laser-induced graphene electrodes for NO2 sensing. *ACS Appl. Nano Mater.* **3**, 2545–2553 (2020).
230. Hou, C., Tai, G., Liu, Y. & Liu, X. Borophene gas sensor. *Nano Res.* **15**, 2537–2544 (2022).
231. Chang, S. L. et al. Intrinsically flexible CNT-TiO2-Interlaced film for NO sensing at room temperature. *Appl. Surface Sci.* **579**, 152172 (2022).
232. Wu, Z. X. et al. A self-powered, rechargeable, and wearable hydrogel patch for wireless gas detection with extraordinary performance. *Adv. Funct. Mater.* **33**, https://doi.org/10.1002/adfm.202300046 (2023).
233. Mahajan, A. & Gasso, S. Self-powered wearable gas sensors based on L-Ascorbate-Treated MXene nanosheets and SnO2 nanofibers. *ACS Appl. Nano Mater.* **6**, 6678–6692 (2023).
234. Li, X. W. et al. Highly flexible all-inorganic nanofiber networks with stress-accommodating microstructure for light-activated wearable chemiresistive sensor. *Chem. Eng. J.* **455**, 140768 (2023).
235. Gao, Z. D. et al. Engineering CuMOF in TiO2 nanochannels as flexible gas sensor for high-performance NO detection at room temperature. *ACS Sens.* **7**, 2750–2758 (2022).
236. Huang, Y. F. et al. Liquid metal-based epidermal flexible sensor for wireless breath monitoring and diagnosis enabled by highly sensitive SnS2 nanosheets. *Research* **2021**, 9847285 (2021).
237. Wang, L. J. et al. Facile synthesis of conductive metal-organic frameworks nanotubes for ultrahigh-performance flexible NO sensors. *Small Methods* **6**, 2200581 (2022).
238. Zang, W. et al. Core-Shell In2O3/ZnO nanoarray nanogenerator as a self-powered active gas sensor with high H2S sensitivity and selectivity at room temperature. *J. Phys. Chem. C* **118**, 9209–9216 (2014).
239. Asad, M. & Sheikhi, M. H. Highly sensitive wireless H2S gas sensors at room temperature based on CuO-SWCNT hybrid nanomaterials. *Sens. Actuators B Chem.* **231**, 474–483 (2016).
240. Kim, S. G., Tran, T. V. & Lee, J. S. Iron oxide-immobilized porous carbon nanofiber-based radio frequency identification (RFID) tag sensor for detecting hydrogen sulfide. *J. Ind. Eng. Chem.* **112**, 423–429 (2022).
241. Wang, J. et al. Ultrathin 2D NbWO6 perovskite semiconductor based gas sensors with ultrahigh selectivity under low working temperature. *Adv. Mater.* **34**, 2104958 (2022).
242. Zhang, X. L. et al. Flexible H2S sensors: Fabricated by growing NO2-UiO-66 on electrospun nanofibers for detecting ultralow concentration H2S. *Appl. Surface Sci.* **573**, 151446 (2022).
243. Zhu, Z. Y. et al. Flexible fiber-shaped hydrogen gas sensor via coupling palladium with conductive polymer gel fiber. *J. Hazardous Mater.* **411**, 125008 (2021).
244. Cho, M., Yun, J., Kwon, D., Kim, K. & Park, I. High-sensitivity and low-power flexible schottky hydrogen sensor based on silicon nanomembrane. *ACS Appl. Mater. Interfaces* **10**, 12870–12877 (2018).
245. Kim, D. H. et al. High-resolution, fast, and shape-conformable hydrogen sensor platform: polymer nanofiber yarn coupled with nanograined Pd@Pt. *ACS Nano* **13**, 6071–6082 (2019).
246. Nair, K. G., Vishnuraj, R. & Pullithadathil, B. Highly sensitive, flexible H-2 gas sensors based on less platinum bimetallic Ni-Pt nanocatalyst-functionalized carbon nanofibers. *ACS Appl. Electron. Mater.* **3**, 1621–1633 (2021).
247. Xie, B. et al. Pd nanoparticle film on a polymer substrate for transparent and flexible hydrogen sensors. *ACS Appl. Mater. Interfaces* **10**, 44603–44613 (2018).
248. Chen, Z. K. et al. Lead-free halide Cs2PtI6 perovskite favoring Pt-N bonding for trace NO detection. *ACS Sens.* **6**, 3800–3807 (2021).
249. Punetha, D., Kar, M. & Pandey, S. K. A new type low-cost, flexible and wearable tertiary nanocomposite sensor for room temperature hydrogen gas sensing. *Sci. Rep.* **10**, 2151 (2020).

250. Huang, X. W. et al. Superhydrophilic, underwater superoleophobic, and highly stretchable humidity and chemical vapor sensors for human breath detection. *ACS Appl. Mater. Interfaces* **11**, 24533–24543 (2019).
251. Hu, L. H. et al. A self-powered sound-driven humidity sensor for wearable intelligent dehydration monitoring system. *Nanotechnology* **34**, 195501 (2023).
252. Wang, J. J., Wang, N., Xu, D., Tang, L. & Sheng, B. Flexible humidity sensors composed with electrodes of laser induced graphene and sputtered sensitive films derived from poly (ether-ether-ketone). *Sens. Actuators B Chem.* **375**, 132846 (2023).
253. Yan, D., Qiu, L. L., Shea, K. J., Meng, Z. H. & Xue, M. Dyeing and functionalization of wearable silk fibroin/cellulose composite by nanocolloidal array. *ACS Appl. Mater. Interfaces* **11**, 39163–39170 (2019).
254. Hou, C. et al. Ultrasensitive humidity sensing and the multifunctional applications of borophene-MoS2 heterostructures. *J. Mater. Chem. A* **9**, 13100–13108 (2021).
255. Park, S. Y. et al. Highly selective and sensitive chemoresistive humidity sensors based on rGO/MoS2 van der Waals composites. *J. Mater. Chem. A* **6**, 5016–5024 (2018).
256. Hou, C., Tai, G. A., Liu, B., Wu, Z. H. & Yin, Y. H. Borophene-graphene heterostructure: preparation and ultrasensitive humidity sensing. *Nano Res.* **14**, 2337–2344 (2021).
257. Noh, W., Go, Y. & An, H. Y. S. Reduced graphene oxide/polyelectrolyte multilayers for fast resistive humidity sensing. *Sensors* **23**, 1977 (2023).
258. Khattak, Z. J., Sajid, M., Javed, M., Rizvi, H. M. Z. & Awan, F. S. Mass-producible 2D nanocomposite-based temperature-independent all-printed relative humidity sensor. *ACS Omega* **7**, 16605–16615 (2022).
259. Yao, D. J. et al. Gas-permeable and highly sensitive, washable and wearable strain sensors based on graphene/carbon nanotubes hybrids e-textile. *Composites Part a Appl. Sci. Manuf.* **149**, 106556 (2021).
260. Guo, Q., Pang, W. W., Xie, X., Xu, Y. L. & Yuan, W. J. Stretchable, conductive and porous MXene-based multilevel structured fibers for sensitive strain sensing and gas sensing. *J. Mater. Chem. A* **10**, 15634–15646 (2022).
261. Gao, W. C. et al. Design of a superhydrophobic strain sensor with a multilayer structure for human motion monitoring. *ACS Appl. Mater. Interfaces* **14**, 1874–1884 (2022).
262. Huang, T. C., et al., Ultralight, elastic, hybrid aerogel for flexible/wearable piezoresistive sensor and solid-solid/gas-solid coupled triboelectric nanogenerator. *Adv. Sci.* **9**, (2022).
263. Sun, S., Hao, F. Y. & Maimaitiyiming, X. 3D print polyaniline/gelatin hydrogels as wearable multifunctional sensors. *Chemistryselect*. **7** (2022).
264. Hu, J. S. et al. Nano carbon black-based high performance wearable pressure sensors. *Nanomaterials* **10**, 664 (2020).
265. Jiang, S. W., Yu, J. T., Xiao, Y., Zhu, Y. Y. & Zhang, W. L. Ultrawide sensing range and highly sensitive flexible pressure sensor based on a percolative thin film with a knoll-like microstructured surface. *ACS Appl. Mater. Interfaces* **11**, 20500–20508 (2019).
266. Yang, T. et al. Hierarchically structured PVDF/ZnO core-shell nanofibers for self-powered physiological monitoring electronics. *Nano Energy* **72**, 104706 (2020).
267. Jiang, D. et al. Superelastic Ti3C2Tx MXene-based hybrid aerogels for compression-resilient devices. *ACS Nano* **15**, 5000–5010 (2021).
268. Chao, M. Y. et al. Breathable Ti3C2Tx MXene/protein nanocomposites for ultrasensitive medical pressure sensor with degradability in solvents. *ACS Nano* **15**, 9746–9758 (2021).
269. Zhou, Q. et al. Lithography-free formation of controllable microdomes via droplet templates for robust, ultrasensitive, and flexible pressure sensors. *ACS Appl. Nano Mater.* **2**, 7178–7187 (2019).
270. Zhang, H. et al. Pillared carbon@tungsten decorated reduced graphene oxide film for pressure sensors with ultra-wide operation range in motion monitoring. *Carbon* **189**, 430–442 (2022).
271. Ren, H. Y. et al. Transfer-medium-free nanofiber-reinforced graphene film and applications in wearable transparent pressure sensors. *ACS Nano* **13**, 5541–5548 (2019).
272. Mondal, S., Min, B. K., Yi, Y., Nguyen, V. T. & Choi, C. G. Gamma-ray tolerant flexible pressure-temperature sensor for nuclear radiation environment. *Adv. Mater. Technol.* **6**, 2001039 (2021).
273. Zhang, J. R. et al. Direct laser patterning of free-standing rgo electrodes for wearable capacitive pressure sensors. *IEEE Photon. Technol. Lett.* **34**, 1361–1364 (2022).
274. Eatemadi, A. et al. Carbon nanotubes: properties, synthesis, purification, and medical applications. *Nanoscale Res. Lett.* **9**, 393 (2014).
275. Kayser, L. V. & Lipomi, D. J. Stretchable conductive polymers and composites based on PEDOT and PEDOT:PSS. *Adv. Mater.* **31**, 1806133 (2019).
276. Naguib, M., Barsoum, M. W. & Gogotsi, Y. Ten years of progress in the synthesis and development of MXenes. *Adv. Mater.* **33**, 2103393 (2021).
277. Vaughan, J. et al. Exhaled breath condensate pH is a robust and reproducible assay of airway acidity. *Eur. Respir. J.* **22**, 889–894 (2003).
278. Mitsubayashi, K. et al. Wearable and flexible oxygen sensor for transcutaneous oxygen monitoring. *Sens. Actuators B Chem.* **95**, 373–377 (2003).
279. Tentzeris, M. M., Nikolaou, S. & IEEE. RFID-enabled ultrasensitive wireless sensors utilizing inkjet-printed antennas and carbon nanotubes for gas detection applications. In *Proc IEEE International Conference on Microwaves, Communications, Antennas and Electronics Systems (Comcas 2009)*, (IEEE Xplore, 2009).
280. Jia, H. Y., Wang, J., Zhang, X. Y. & Wang, Y. P. Pen-writing polypyrrole arrays on paper for versatile cheap sensors. *ACS Macro Lett.* **3**, 86–90 (2014).
281. Zheng, Z. Q., Yao, J. D., Wang, B. & Yang, G. W. Light-controlling, flexible and transparent ethanol gas sensor based on ZnO nanoparticles for wearable devices. *Sci. Rep.* **5**, 11070 (2015).
282. Kang, M. A. et al. Highly sensitive and wearable gas sensors consisting of chemically functionalized graphene oxide assembled on cotton yarn. *RSC Adv.* **8**, 11991–11996 (2018).
283. Shiu, B. C., Liu, Y. L., Yuan, Q. Y., Lou, C. W. & Lin, J. H. Preparation and characterization of PEDOT:PSS/TiO2 micro/nanofiber-based gas sensors. *Polymers* **14**, 1780 (2022).
284. Lee, T. et al. Large-area synthesis of ultrathin, flexible, and transparent conductive metal-organic framework thin films via a microfluidic-based solution shearing process. *Adv. Mater.* **34**, 2107696 (2022).
285. Lee, K. et al. Rough-surface-enabled capacitive pressure sensors with 3D touch capability. *Small* **13**, 1700368 (2017).
286. Haick, H., Broza, Y. Y., Mochalski, P., Ruzsanyi, V. & Amann, A. Assessment, origin, and implementation of breath volatile cancer markers. *Chem. Soc. Rev.* **43**, 1423–1449 (2014).